Article

Cell Stem Cell

Inflammation-Induced Emergency Megakaryopoiesis Driven by Hematopoietic Stem Cell-like Megakaryocyte Progenitors

Graphical Abstract

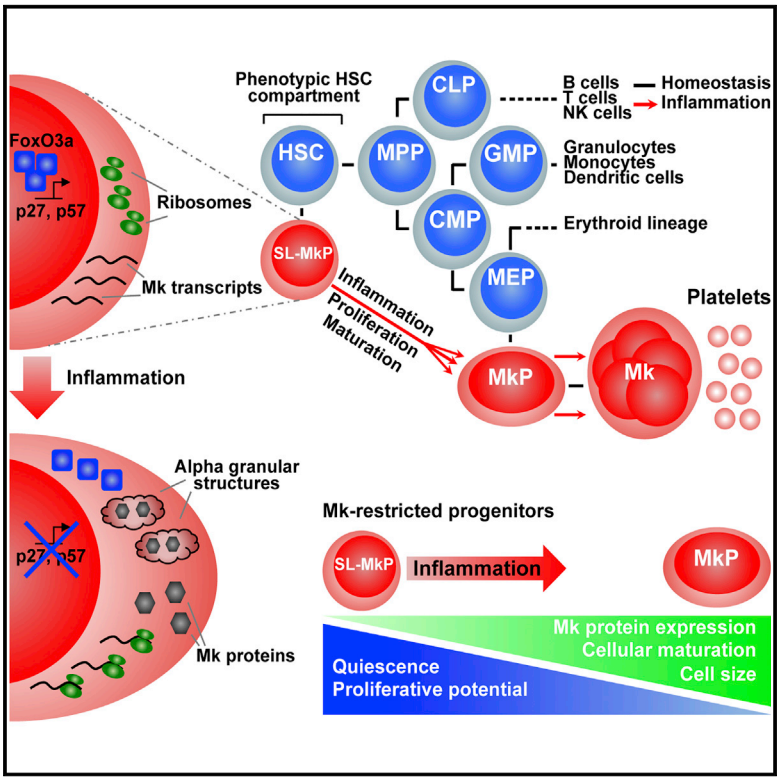

Highlights

- Unipotent SL-MkPs are maintained in a quiescent, but primed, state during homeostasis
- Inflammation instructs post-transcriptional Mk protein synthesis in SL-MkPs
- Inflammation drives efficient cell cycle activation and maturation of SL-MkPs
- Activation of SL-MkPs rapidly replenishes the platelet pool during acute inflammation

Authors

Simon Haas, Jenny Hansson, Daniel Klimmeck, ..., Andreas Trumpp, Jeroen Krijgsveld, Marieke A.G. Essers

Correspondence

m.essers@dkfz.de

In Brief

Haas et al. show that inflammatory signaling activates post-transcriptional protein synthesis, maturation, and cell cycle induction in quiescent, but primed, stem-like megakaryocyte progenitors. This emergency program efficiently prevents otherwise life-threatening platelet depletion during acute inflammation.

Accession Numbers

GSE64002

Haas et al., 2015, Cell Stem Cell *17*, 422–434
October 1, 2015
http://dx.doi.org/10.1016/j.stem.2015.07.007

CellPress

Cell Stem Cell
Article

Inflammation-Induced Emergency Megakaryopoiesis Driven by Hematopoietic Stem Cell-like Megakaryocyte Progenitors

Simon Haas,[1,2] Jenny Hansson,[3,13] Daniel Klimmeck,[1,3,4] Dirk Loeffler,[5] Lars Velten,[3] Hannah Uckelmann,[1,2] Stephan Wurzer,[1,2] Áine M. Prendergast,[1,2] Alexandra Schnell,[1,2] Klaus Hexel,[6] Rachel Santarella-Mellwig,[7] Sandra Blaszkiewicz,[1,2] Andrea Kuck,[1,2] Hartmut Geiger,[8,9] Michael D. Milsom,[1,10] Lars M. Steinmetz,[3,11,12] Timm Schroeder,[5] Andreas Trumpp,[1,4] Jeroen Krijgsveld,[3] and Marieke A.G. Essers[1,2,*]

[1]Heidelberg Institute for Stem Cell Technology and Experimental Medicine (HI-STEM gGmbH), 69120 Heidelberg, Germany
[2]Division of Stem Cells and Cancer, Hematopoietic Stem Cells and Stress Group, Deutsches Krebsforschungszentrum (DKFZ), 69120 Heidelberg, Germany
[3]European Molecular Biology Laboratory (EMBL), Genome Biology Unit, 69117 Heidelberg, Germany
[4]Division of Stem Cells and Cancer, Deutsches Krebsforschungszentrum (DKFZ), 69120 Heidelberg, Germany
[5]Department of Biosystems Science and Engineering (D-BSSE), ETH Zurich, 4058 Basel, Switzerland
[6]Core Facility Flow Cytometry, Deutsches Krebsforschungszentrum (DKFZ), 69120 Heidelberg, Germany
[7]European Molecular Biology Laboratory (EMBL), Electron Microscopy Core Facility, 69117 Heidelberg, Germany
[8]Institute for Molecular Medicine, Ulm University, 89081 Ulm, Germany
[9]Division of Experimental Hematology and Cancer Biology, Cincinnati Children's Hospital Medical Center and University of Cincinnati, Cincinnati, OH 45229, USA
[10]Division of Stem Cells and Cancer, Experimental Hematology Group, Deutsches Krebsforschungszentrum (DKFZ), 69120 Heidelberg, Germany
[11]Stanford Genome Technology Center, Palo Alto, CA 94304, USA
[12]Department of Genetics, Stanford University School of Medicine, Stanford, CA 94305, USA
[13]Present address: Division of Molecular Hematology, Lund Stem Cell Center, Lund University, 221 84 Lund, Sweden
*Correspondence: m.essers@dkfz.de
http://dx.doi.org/10.1016/j.stem.2015.07.007

SUMMARY

Infections are associated with extensive platelet consumption, representing a high risk for health. However, the mechanism coordinating the rapid regeneration of the platelet pool during such stress conditions remains unclear. Here, we report that the phenotypic hematopoietic stem cell (HSC) compartment contains stem-like megakaryocyte-committed progenitors (SL-MkPs), a cell population that shares many features with multipotent HSCs and serves as a lineage-restricted emergency pool for inflammatory insults. During homeostasis, SL-MkPs are maintained in a primed but quiescent state, thus contributing little to steady-state megakaryopoiesis. Even though lineage-specific megakaryocyte transcripts are expressed, protein synthesis is suppressed. In response to acute inflammation, SL-MkPs become activated, resulting in megakaryocyte protein production from pre-existing transcripts and a maturation of SL-MkPs and other megakaryocyte progenitors. This results in an efficient replenishment of platelets that are lost during inflammatory insult. Thus, our study reveals an emergency machinery that counteracts life-threatening platelet depletions during acute inflammation.

INTRODUCTION

The continuous production of blood and immune cells is regulated by a small number of multipotent and self-renewing hematopoietic stem cells (HSCs) residing in the bone marrow of adult mammals (Orkin and Zon, 2008). In response to bone marrow injury or infection, long-term quiescent HSCs are efficiently recruited into the cell cycle and return back to quiescence after re-establishment of homeostasis (Baldridge et al., 2010; Essers et al., 2009; Wilson et al., 2008). Positioned at the apex of the hierarchically organized hematopoietic system, HSCs generate a series of progenitor cells that undergo several consecutive commitment steps, becoming progressively restricted in their lineage potential and finally producing unipotent progenitors (Orkin and Zon, 2008). Megakaryocytes (Mks) are large, polyploid cells that release platelets into the circulation (Machlus and Italiano, 2013). According to the classical model of hematopoiesis, each mature Mk derives from an HSC that sequentially transitioned through the multipotent progenitor (MPP), common myeloid progenitor (CMP), Mk-erythroid progenitor (MEP), and Mk progenitor (MkP) states, followed by endomitosis to generate a mature Mk (Machlus and Italiano, 2013). However, the first evidence for a potential bypass of some intermediate states from HSCs toward Mks was provided when transcriptional profiling revealed expression of Mk transcripts in highly purified HSCs (Månsson et al., 2007). More recently, mRNA expression of the Mk marker von Willebrand factor (*Vwf*) and the surface receptor c-Kit were suggested to be indicative of a platelet-biased, but multipotent

HSC sub-population (Sanjuan-Pla et al., 2013; Shin et al., 2014). Moreover, the existence of Mk-lineage restricted cells with high self-renewal activity in the phenotypic HSC compartment was proposed based on single-cell transplantation experiments (Yamamoto et al., 2013). However, a molecular and cellular characterization of these potent Mk-restricted cells is lacking and the purpose of Mk-lineage priming effects and potential physiological benefits of shortcuts into the Mk lineage remain unclear.

Recent reports highlight the importance of platelets as inflammatory and immune cells in addition to their well-known function in thrombosis (Semple et al., 2011; Yeaman, 2014). Systemic inflammation associated with acute infections triggers the release of immunomodulatory agents and the interaction of platelets with neutrophils to facilitate the formation of neutrophil extracellular traps (NETs) (Jenne et al., 2013; Yeaman, 2014). This provokes a rapid consumption of platelets, resulting in a transient thrombocytopenia (Stohlawetz et al., 1999; Tacchini-Cottier et al., 1998). During acute inflammation, low platelet levels are associated with a loss of vascular integrity and hemorrhage, as well as septic shock, resulting in increased mortality (Goerge et al., 2008; Xiang et al., 2013). Therefore, a fast recovery of platelet levels is essential. However, the exact mechanism by which platelet levels are rapidly regenerated after acute inflammation remains unknown.

Here, we report the existence of potent stem-like Mk-committed progenitors (SL-MkPs) within the phenotypic HSC compartment. Under stress conditions like viral infections, acute inflammatory signaling triggers cell cycle activation of quiescent SL-MkPs and Mk protein production, which drives a rapid maturation program of SL-MkPs and other MkPs. Together, this mediates an efficient platelet recovery after inflammation-induced thrombocytopenia.

RESULTS

Inflammatory Signaling Drives Megakaryocytic Protein Expression in Phenotypic HSCs

Inflammatory signaling during infection triggers a rapid depletion of circulating platelets and other blood cells. To study the hematopoietic system during such stress conditions, we mimicked a viral infection by inducing acute inflammation through administration of a single dose of polyinosinic:polycytidylic acid (pI:C) to mice. As expected, inflammation was associated with dramatic reduction in platelet numbers, but homeostatic blood platelet levels were restored within a few days, suggesting intensive platelet regeneration (Figure 1A). To elucidate which cell types might be involved in this rapid platelet regeneration program, we measured the expression of CD41 (Itga2b), an early marker of megakaryocytic maturation, in distinct cell populations of the hematopoietic stem and progenitor cell compartment during homeostasis and 16 hr after pI:C induction (see Supplemental Information; Figures S1A–S1C for gating strategies under inflammation). In accordance with previous reports, CD41 was expressed in MkPs and at low levels in a subset of HSCs during homeostasis (Gekas and Graf, 2013). Unexpectedly, all investigated cell types potentially capable of generating Mks robustly increased CD41 protein expression upon pI:C treatment, including MkPs, MEPs, and, most surprisingly, phenotypic HSCs, whereas other cell types remained unaffected (Figure 1B). Since inflammation induced the strongest relative upregulation of CD41 in the HSC compartment, we subjected fluorescence activated cell sorting (FACS) purified HSCs ($Lin^-cKit^+CD150^+CD48^-$) and progenitors ($Lin^-cKit^+CD150^+CD48^+$) from control and pI:C treated mice to mass spectrometry-based quantitative proteomics in order to globally characterize inflammation-mediated changes in the HSC proteome. Of a total of 7,492 identified proteins, 162 proteins were significantly changed in HSCs upon induction of inflammation (Table S1). As expected, pI:C treatment triggered the production of typical interferon (IFN) response proteins (Figures 1C, 1D, S1D, and S1E), but also revealed a significant increase of 28 proteins typically expressed in mature Mks and platelets (Figures 1C, 1D, and S1E). These included CD41 (Itga2b) and its partner CD61 (Itgb3), components of the GPIb-IX-V complex, platelet-selectin (Selp), the platelet and Mk-specific β1 tubulin (Tubb1), as well as many proteins characteristic for Mk and platelet alpha-granules, such as Vwf and platelet factor 4 (Pf4). In concert with our finding that inflammation-driven Mk protein increase is highest in HSCs (Figure 1B), the upregulation of Mk proteins in $Lin^-cKit^+CD150^+CD48^+$ progenitors was almost absent (Figures 1C, 1D, S1E, and S1F).

Since pI:C administration triggers a wide production and secretion of type-I IFNs in vivo, we hypothesized that type-I IFN signaling might be involved in regulating the production of Mk proteins in HSCs. Accordingly, administration of recombinant IFNα phenocopied pI:C injections with regards to Mk protein upregulation (Figure S1G), and the pI:C-mediated increase in Mk proteins was completely absent in HSCs from IFNα receptor (IFNAR) knockout mice (Figures 1D and S1E). The analysis of forward, reverse, and 50:50 wild-type (WT):$IFNAR^{-/-}$ bone marrow chimeras revealed that type-I IFN signaling directly instructs Mk protein expression in phenotypic HSCs (Figure S1H). Canonical type-I IFN signaling results in the activation of the signal transducer STAT1 and crosstalk signaling to mTOR has been reported (Platanias, 2005). Therefore, we investigated the involvement of STAT1 and mTOR in pI:C-mediated Mk protein upregulation. Either the pharmacological inhibition of mTOR using rapamycin or the genetic deletion of STAT1 reduced inflammation-mediated Mk protein upregulation, suggesting that both pathways participate in the regulation of Mk protein production in HSCs (Figures S1I–S1K). In contrast, stem cell antigen 1 (Sca-1), involved in pI:C-induced cell cycle activation of HSCs, was not required for pI:C-induced Mk protein expression (Figure S1L). Moreover, single administrations of lipopolysaccharide (LPS), mimicking a bacterial infection, or recombinant tumor necrosis factor alpha (TNFα), a cytokine involved in mediating acute inflammation, also triggered an increase of Mk proteins in HSCs comparable to pI:C (Figure 1E). In contrast to pI:C, LPS-mediated Mk protein expression in HSCs was mediated by TLR4/MYD88/TRIF-signaling (Figure S1M). Reducing platelet levels using a platelet depletion antibody without triggering inflammation induced only a minor increase of Mk proteins, further highlighting the importance of inflammatory signaling (Figure S1N). Together, these data demonstrate that inflammatory signaling associated with infections directly triggers Mk protein expression in phenotypic HSCs.

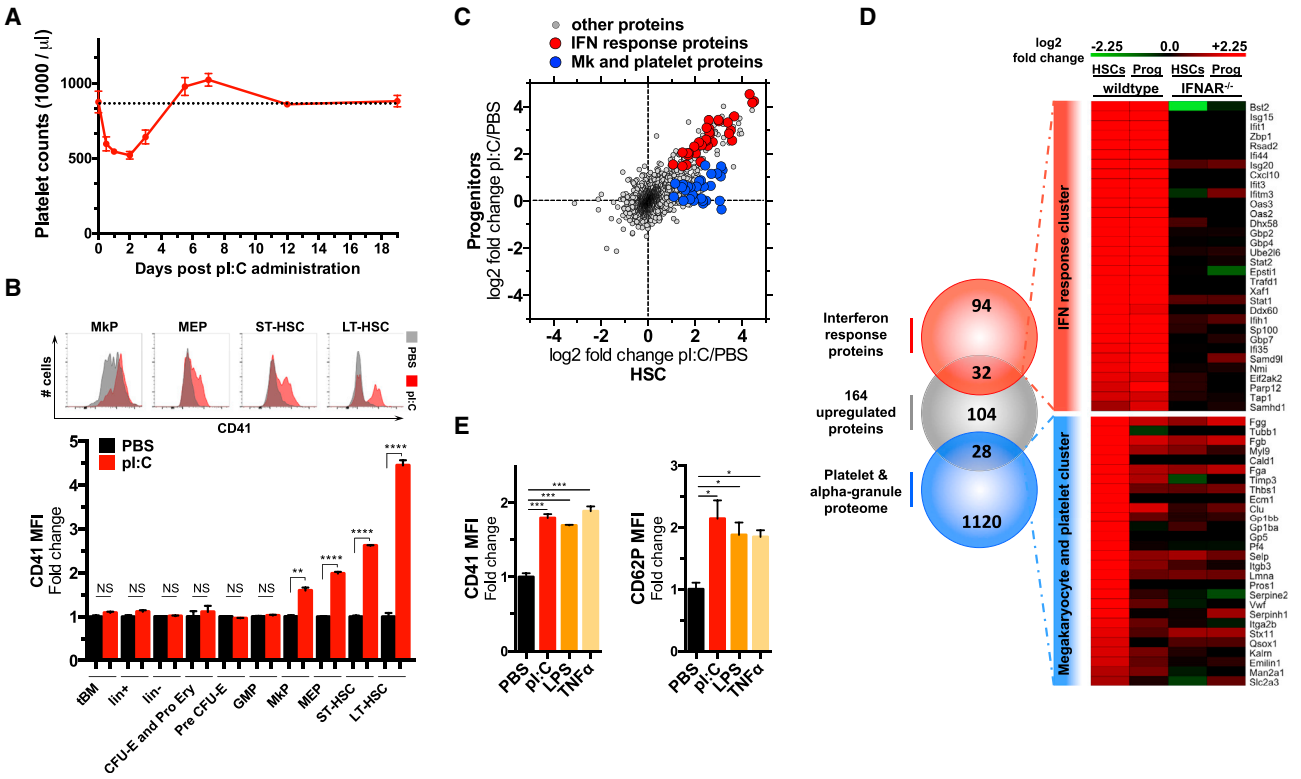

Figure 1. Inflammation Drives Megakaryocytic Protein Expression in HSCs

(A) Platelet counts upon treatment with pI:C.

(B) Flow cytometric analysis of CD41 expression in distinct stem and progenitor compartments of PBS and pI:C treated mice 16 hr after injection.

(C and D) Mass spectrometry-based quantitative proteome analysis of HSCs ($Lin^-cKit^+CD150^+CD48^-$) and progenitors ($Lin^-cKit^+CD150^+CD48^+$) isolated from WT and $IFNAR^{-/-}$ mice 16 hr after PBS or pI:C treatment.

(C) Scatter plot of fold changes in protein levels upon pI:C treatment in HSCs and progenitors of WT mice.

(D) Heatmap illustrating protein log2 fold changes upon pI:C treatment in WT and $IFNAR^{-/-}$ HSCs and progenitors for the overlapping proteins of the Venn diagram.

(E) Flow cytometric analysis of CD41 and CD62P expression in HSCs 16 hr after pI:C, LPS and TNFα administration.

In (A), (B), and (E), data are presented as mean ± SEM with $n \geq 3$. The significance was determined using an unpaired, two-tailed student's t test (*$p \leq 0.05$, **$p \leq 0.01$, ***$p \leq 0.001$, ****$p \leq 0.0001$, and non-significant: NS). See also Figure S1.

SL-MkPs within the Phenotypic HSC Compartment Increase Mk Protein Expression upon Acute Inflammation

Recent reports identified multipotent HSCs with intrisinc Mk bias as well as unipotent Mk-committed progenitors in the phenotypic HSC compartment (Sanjuan-Pla et al., 2013; Shin et al., 2014; Yamamoto et al., 2013). To determine whether inflammation-driven Mk protein expression takes place primarily in multipotent HSCs or in other cell types present in the phenotypic HSCs compartment and to investigate whether elevated Mk protein levels are associated with Mk lineage fate decisions, we made use of high-throughput single-cell ex vivo lineage tracking (Figure 2A). Single LT-HSCs were sorted into differentiation medium containing fluorescently labeled antibodies, and the morphology and expression of lineage makers of individual cells was tracked in clonally expanded progeny by daily fluorescence microscopy. This allowed a time-resolved analysis of ex vivo differentiation in a quantitative manner. As expected, the majority of HSCs from homeostatic mice formed large "*mixed*" colonies containing both myeloid and megakaryocytic cells. However, a fraction of the phenotypic HSCs generated exclusively mature Mks, suggesting that these cells were committed to Mk-lineage (Figures 2B, S2A, and S2B). This sets them apart from multipotent, but Mk-biased, populations such as *Vwf*$^+$ HSCs (Sanjuan-Pla et al., 2013), but is in accordance with a recent single-cell transplantation study identifying Mk-committed progenitors with high self-renewal potential in the HSC compartment (Yamamoto et al., 2013). While some phenotypic HSCs directly gave rise to single Mks, others formed large colonies consisting of up to hundreds of mature Mks (Figures S2A and S2B). These potent stem cell-like megakaryocyte-committed progenitors (SL-MkPs) are distinct to classical MkPs and exist within the phenotypic HSC pool during homeostasis (Figures S2A and S2B). The number of single-sorted HSCs giving rise to "*Mk only*" colonies during homeostasis and inflammation was the same (Figure 2B), suggesting that commitment of multipotent HSCs to SL-MkPs occurs during homeostasis, and inflammatory signaling induces Mk protein expression without affecting lineage fate decisions. To determine which cell types increase Mk protein levels upon inflammation, we retrospectively assigned CD41 fluorescence intensity values

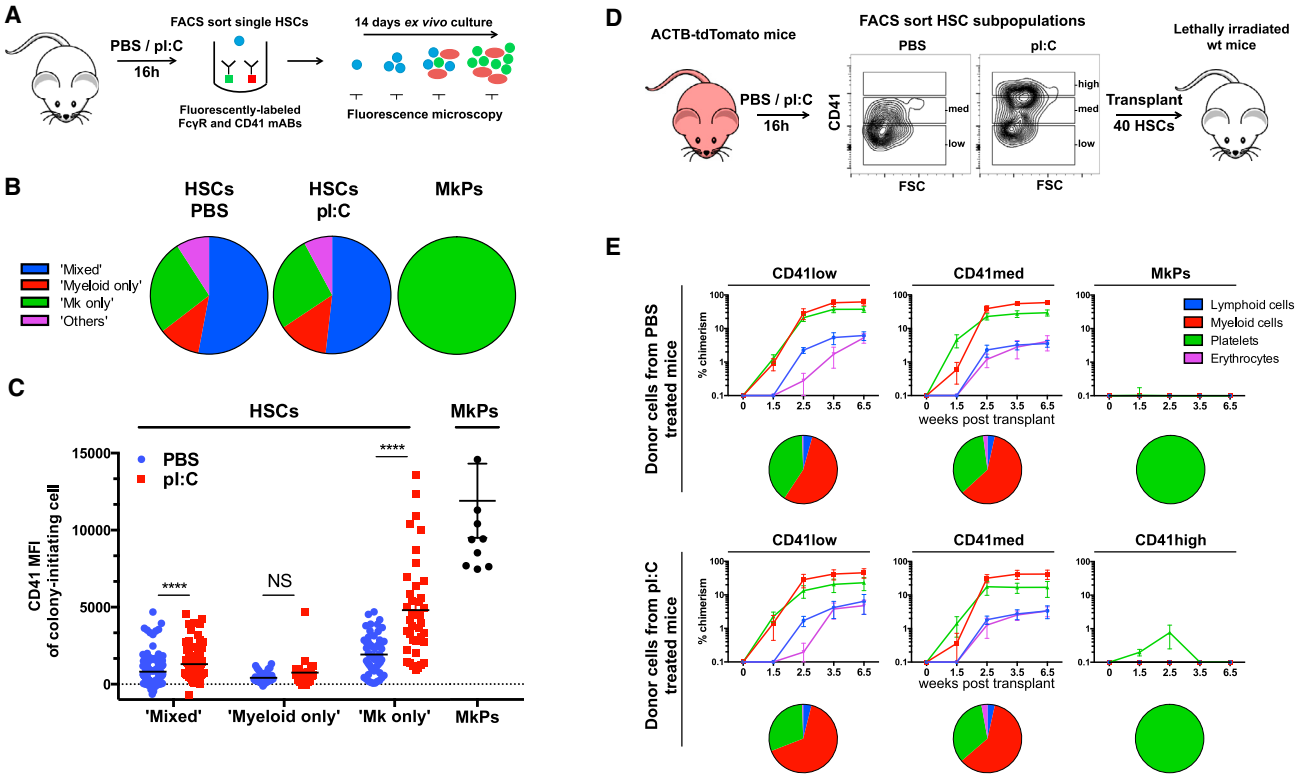

Figure 2. Stem-like Mk-Committed Progenitors within the Phenotypic HSC Compartment Increase Mk Protein Levels upon Acute Inflammation

(A–C) Ex vivo lineage tracking of single LT-HSCs from PBS and pI:C treated mice. The representative data for one out of two independently performed experiments is shown. (A) Illustration of experimental approach. (B) Distribution of colony types formed at day 14 of ex vivo liquid culture. (C) CD41 surface expression of single-sorted LT-HSCs and MkPs giving rise to the indicated colony types.

(D and E) Transplantation of LT-HSC CD41 sub-populations. The ACTB-Tomato mice were treated with PBS or pI:C, after 16 hr, 40 LT-HSCs or 300 MkPs were transplanted into lethally irradiated WT recipients. (D) Illustration of experimental approach. (E) Results. The pie charts represent relative lineage contributions. For (C) and (E), the data are presented as mean ± SEM. The significance was determined using a Mann-Whitney-Wilcoxon test (*p ≤ 0.05, **p ≤ 0.01, ***p ≤ 0.001, ****p ≤ 0.0001, and non-significant: NS). See also Figure S2.

from single-sorted HSCs to the colony types they formed (Figure 2C). Phenotypic HSCs generating mixed colonies showed minor, but significant, increase in CD41 expression upon inflammation, whereas cells generating "*myeloid only*" colonies remained unaffected from CD41 upregulation. In contrast, SL-MkPs (i.e., cells giving rise to Mk only colonies) robustly increased CD41 expression to elevated levels upon inflammation, suggesting that SL-MkPs are the primary source of Mk protein expression upon pI:C treatment within the phenotypic HSC compartment.

To confirm this finding in vivo, we sub-fractionated LT-HSCs from ACTB-tdTomato mice based on their CD41 signal into CD41*low* and *med* for PBS treated mice and CD41*low*, *med*, and *high* for pI:C treated mice and traced the generation of tomato-positive lineage cells in the blood (Figures 2D and 2E). In line with our single-cell ex vivo data, CD41*low* and CD41*med* HSCs from both PBS and pI:C treated mice showed multilineage reconstitution (Gekas and Graf, 2013), whereas CD41*high* HSCs from pI:C treated mice exclusively generated platelets in a transient manner, demonstrating that these cells were committed to the Mk lineage (Figure 2E). In contrast, MkPs generated a much lower platelet chimerism, confirming that CD41*high* HSCs represent potent SL-MkPs that are superior to classical MkPs in their platelet generation capacity. Together, these data demonstrate that commitment of HSCs to SL-MkPs appears during homeostasis. While SL-MkPs express similar levels of Mk proteins compared to HSCs during homeostasis, inflammatory signaling triggers Mk protein expression in SL-MkPs without affecting lineage commitment of HSCs to SL-MkPs.

Inflammation Drives Functional and Cellular Maturation of SL-MkPs and MkPs

To investigate whether increased Mk protein expression might be attributed to an inflammation-driven maturation of SL-MkPs, we performed kinetic analyses of Mk generation ex vivo. While single-sorted control MkPs did not expand, form small Mk colonies, and mature within the first 2–3 days in culture, SL-MkPs (phenotypic HSCs generating Mk only colonies) from homeostatic mice expanded in an immature state until day 7–8, matured late, and formed large Mk colonies (Figures 3A, S2B, and S2C). In contrast, SL-MkPs from pI:C treated mice generated mature Mks much faster (Figures 3A and S2C), suggesting that inflammation triggered efficient maturation of SL-MkPs. The induced maturation of SL-MkPs was associated with a reduced expansion of immature cells and thus with a

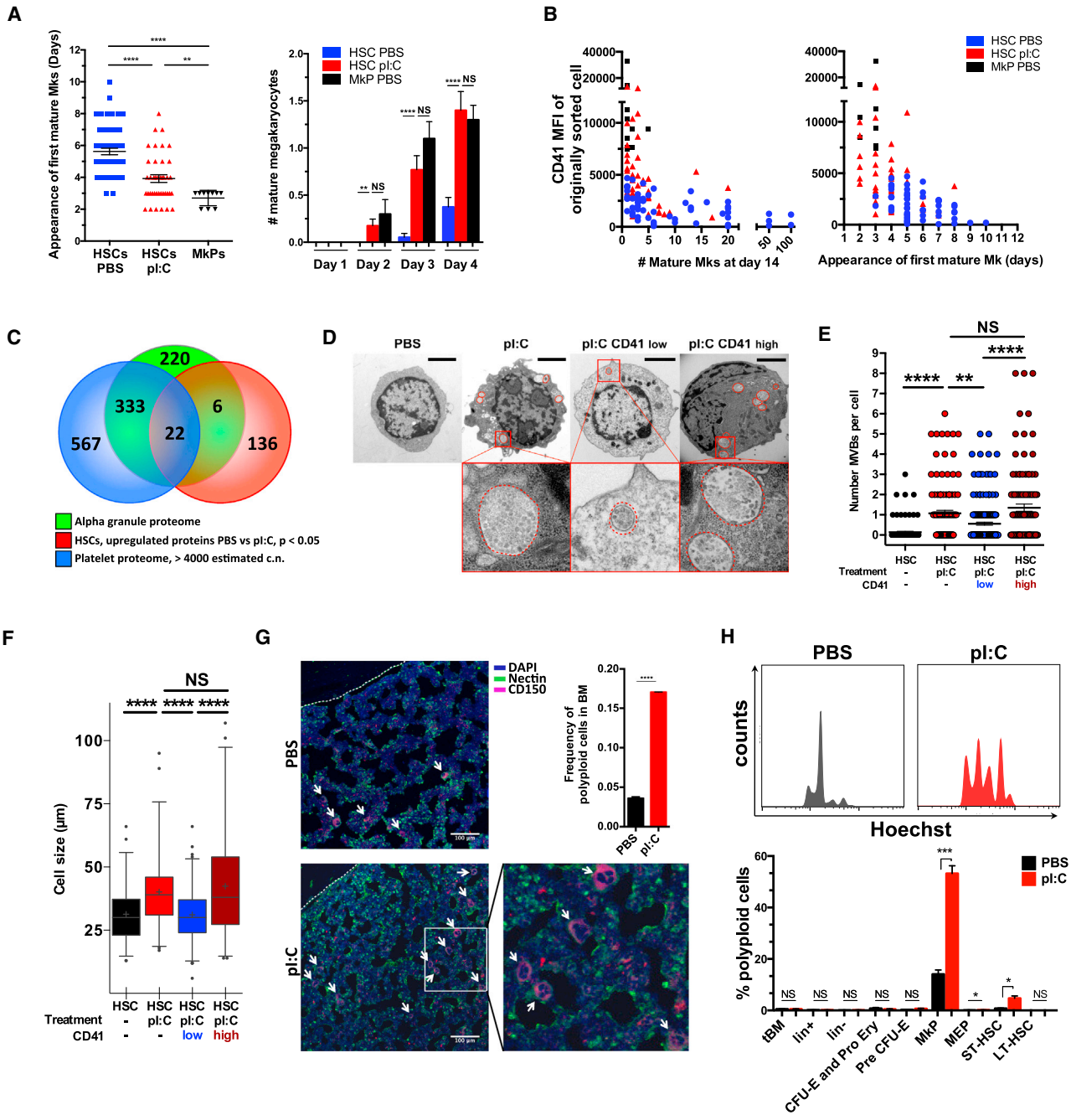

Figure 3. Inflammation Drives a Cellular Mk Maturation Program at Distinct Levels of Megakaryopoiesis

(A) Time until first mature Mk cell appears in the culture of Mk only colonies (left). The mean number of mature Mks at day 1–4 after culture of Mk only colonies (right).

(B) Mk colony size (left) and Mk maturation time (right) of Mk only colonies anti-correlate with CD41 protein expression of originally sorted LT-HSCs (i.e., SL-MkPs). The Mk colony size was determined on day 14 of culture.

(C) Venn diagram illustrating that Mk proteins upregulated in HSCs upon inflammation are typically localized to alpha-granules in platelets.

(D) Electron microscopy visualization of HSCs, CD41low, and CD41high HSCs from PBS and pI:C treated mice 16 hr after treatment. The MVBs are marked in red.

(E) Quantification of MVBs.

(F) Quantification of cell size based on stereology analysis of electron micrographs.

(G) Bone sections and quantification of polyploid Mks. The bone sections were stained with CD150 (red), Nectin (green), and DAPI (blue) 16 hr after treatment. The polyploid Mks were quantified using Hoechst staining and FACS.

(H) Quantification of polyploidy in stem and progenitor cell populations 16 hr after PBS and pI:C treatment. The representative histogram of MkPs is shown at the top. In (A), (E), (G), and (H), data are presented as mean ± SEM with n ≥ 3. The significance was determined using a Mann-Whitney-Wilcoxon test (A and E), or an unpaired, two-tailed student's t test (G and H) (*p ≤ 0.05, **p ≤ 0.01, ***p ≤ 0.001, ****p ≤ 0.0001, and non-significant: NS). See also Figure S3.

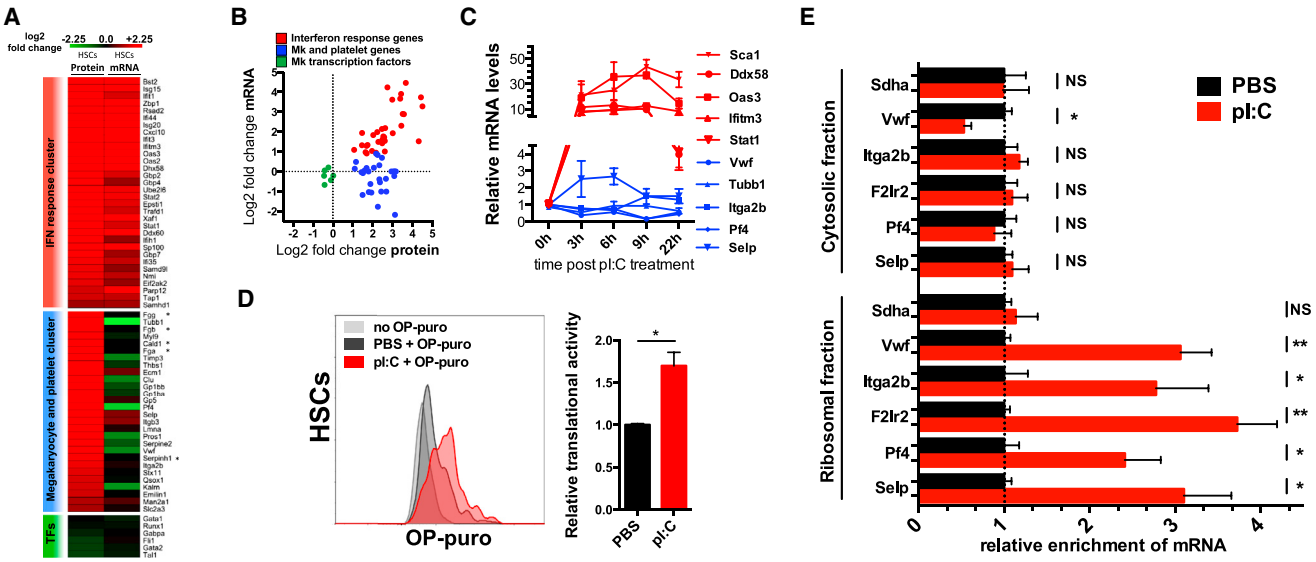

Figure 4. Megakaryocytic Protein Upregulation in HSCs Is Mediated by a Post-Transcriptional Mechanism

(A) Comparison of log2 fold changes in protein level and transcript level of HSCs, isolated from PBS and pI:C treated mice, 16 hr after treatment. The protein and transcript levels derived from proteomics and qPCR, respectively. The genes marked with asterisks were not detected on transcript level.

(B) Scatterplot view from data presented in (A).

(C) Time-course qPCR analysis of Mk (blue) and IFN response gene (red) transcripts at indicated time points after treatment with pI:C in HSCs.

(D) Translational activity of HSCs upon inflammation. The OP-Puro incorporation was measured 16 hr after PBS/pI:C and 1.5 hr after OP-Puro administration (see Supplemental Information).

(E) Ribosomal profiling of Mk transcripts upon inflammation. The mRNA levels of housekeeping (Sdha) and Mk genes (others) were measured in both fractions and normalized to Actb.

In (C)–(E), data are presented as mean ± SEM with $n \geq 3$. The significance was determined using an unpaired, two-tailed student's t test (*$p \leq 0.05$, **$p \leq 0.01$, ***$p \leq 0.001$, ****$p \leq 0.0001$, and non-significant: NS). See also Figure S4.

smaller overall size of Mk colonies (Figure S2C). Interestingly, CD41 expression of the colony-initiating SL-MkPs and MkPs was anti-correlative with both the expansion potency of the cell and with the time required to generate the first mature Mk (Figure 3B). Hence, the most primitive SL-MkPs with low Mk protein expression generate the largest Mk colonies at late time points, while cells with high Mk protein expression generate smaller Mk colonies at early time points. In contrast to SL-MkPs, inflammation had no impact on Mk maturation time or the overall amount of mature Mks generated from HSCs with mixed colony potential (Figure S2C).

Alpha granules or their precursors in the form of multivesicular bodies (MVBs) are typical features of megakaryocytic maturation (Heijnen et al., 1998). Comparison of Mk proteins that were synthesized upon inflammation in HSCs with the platelet alpha-granule proteome (Browne et al., 2001) revealed that the majority of these proteins are typically localized to alpha granules (Figure 3C). In accordance with this, electron microscopy and immunofluorescence microscopy of purified HSCs revealed the generation of MVB-like structures 16 hr after induction of inflammation, which was correlated with the upregulation of Mk proteins and was a particularly frequent event in CD41^{high} SL-MkPs (Figures 3D, 3E, and S3A–S3C). Electron microscopy and FACS analysis revealed an IFNAR-STAT1 and mTOR dependent cell size increase of HSCs, which was particularly attributed to SL-MkPs that upregulate Mk proteins (Figures 3F, S3D, and S3E).

Polyploidy is a characteristic feature of terminally maturated Mks (Machlus and Italiano, 2013). A strong increase in the number of polyploid Mks was observed 16 hr after pI:C treatment (Figure 3G). Quantifying ploidy levels in stem and progenitor cell populations revealed that, in particular, MkPs were driven into endomitosis in an IFNAR-STAT1 dependent manner, whereas phenotypic LT-HSCs did not enter endomitosis (Figures 3H and S3F). Together, these data suggest that inflammation drives a rapid and efficient cellular maturation program of both SL-MkPs and MkPs. SL-MkPs are maintained in a highly potent and primitive state during homeostasis, but are efficiently pushed toward maturation upon inflammation, adapting an intermediate state between homeostatic SL-MkPs and classical MkPs. In contrast to classical MkPs, which are driven into endomitosis forming mature Mks, SL-MkPs are pushed toward maturation without directly undergoing endomitosis, thereby maintaining their high proliferative expansion capacity.

Inflammation-Driven Upregulation of Megakaryocytic Proteins in Phenotypic HSCs Is Mediated by a Post-Transcriptional Mechanism

To determine whether the increase in Mk proteins is transcriptionally controlled, we compared transcript and protein levels of HSCs 16 hr after induction of inflammation. As expected, IFN response genes were regulated at the transcriptional level with a high induction of transcripts, resulting in enhanced protein production (Figures 4A, 4B, and S4A) (Platanias, 2005). In contrast, Mk genes remained unchanged or were even downregulated at the transcriptional level, while the corresponding proteins were significantly increased (Figures 4A, 4B,

and S4A), suggesting a pI:C-induced non-transcriptional regulation of Mk protein expression. In accordance with this, transcription factors regulating Mk gene transcription remained unaffected at the transcript and protein level (Figures 4A, 4B, and S4A). Time course experiments demonstrated a rapid transcriptional induction of IFN response genes, whereas Mk transcripts showed no or only minor increase, excluding the possibility of elevated protein levels caused by an early transcriptional induction of Mk genes (Figure 4C). Several scenarios are conceivable to explain such a non-transcriptional increase in Mk proteins. Whole platelets, or platelet-derived microparticles (PMPs) containing Mk proteins, may adhere to or be taken up by HSCs. However, antibody-mediated depletion of platelets did not affect pI:C-mediated Mk protein increase, suggesting that Mk proteins were not of platelet origin (Figure S4B). Since most Mk transcripts were detected at high levels in HSCs, we reasoned that inflammation-mediated Mk protein production might be a result of increased translation of transcripts that are already present during homeostasis. To measure global levels of translation in phenotypic HSCs, we made use of an O-propargyl-puromycin (OP-Puro)-based method, which facilitates the measurement of translational rates on single-cell level in vivo (Liu et al., 2012; Signer et al., 2014). In accordance with a recent study, homeostatic HSCs showed very low levels of translational activity (Signer et al., 2014), but had significantly increased translational rates upon pI:C treatment (Figure 4D). Importantly, increased translational activity correlated with enhanced Mk protein expression (Figure S4C). In accordance with an enhanced translational activity, phenotypic HSCs demonstrated reduced levels of the translation inhibitors Pdcd4 and Eef2k upon pI:C treatment, which negatively regulate the translation initiation and elongation factors Eif4a and Eef2 (Dorrello et al., 2006; Kruiswijk et al., 2012) (Figure S4D). Occupancy of transcripts at ribosomes is a strong indication of translational activity (Ingolia et al., 2012). Accordingly, Mk transcript occupancy at ribosomes significantly increased upon induction of inflammation, suggesting enhanced translation of these transcripts (Figures 4E and S4E). Together, these experiments suggest that even though most Mk transcripts are expressed in phenotypic HSCs, translation of these transcripts is repressed during homeostasis. In contrast, pI:C treatment instructs efficient translation, resulting in an enhanced Mk protein production.

SL-MkP Commitment Is Associated with a Coordinated Mk Transcription Program Providing Transcriptional Templates for Inflammation-Driven Protein Synthesis

Even though high expression of Mk transcripts in phenotypic HSCs has been well documented (Gekas and Graf, 2013; Månsson et al., 2007; Sanjuan-Pla et al., 2013), the mechanistic role of transcriptional priming is poorly understood. Our data suggest that Mk transcripts are expressed during homeostasis and serve as a template for an efficient inflammation-induced emergency Mk protein synthesis program in SL-MkPs. According to this model, high expression of Mk transcripts in SL-MkPs would be required for mounting an efficient inflammation-mediated post-transcriptional increase in Mk proteins, whereas low Mk transcriptional priming in HSCs would explain their attenuated response.

To characterize Mk lineage priming in HSCs, SL-MkPs, and classical MkPs, we measured Mk and control transcripts of individual MkPs and CD41 sub-populations of LT-HSCs from PBS and pI:C treated mice by single-cell quantitative (q)PCR. In accordance with a previous report, all investigated Mk transcripts were expressed in a bimodal fashion in HSCs, with Cycle-threshold differences (ΔCt) of 15-20 between high-expressing cells and low-expressing cells, suggesting that Mk transcripts are expressed in an "ON" or "OFF" state (Figure 5A) (Guo et al., 2013). Heatmap representation and principal component analysis (PCA) of this data revealed that all MkPs expressed Mk transcripts to high homogenous levels, whereas most LT-HSCs with homeostatic CD41 levels (CD41*low/med* HSCs) expressed a unique combination of Mk transcripts in the ON or OFF state. This was reflected in a funnel-shaped cloud, with each cell occupying a unique location in our PCA analysis, suggesting a stochastic Mk transcript expression (Figures 5B and 5C). Interestingly, some homeostatic LT-HSCs clustered together at the tip of the funnel, representing cells with a coordinated Mk transcription profile with all Mk transcripts in the ON state. Of note, almost all CD41*high* HSCs from pI:C treated mice (i.e., SL-MkPs) expressed all Mk transcripts in the ON state and clustered together with these cells at the tip of the funnel (Figures 5B–5D), demonstrating that homeostatic SL-MkPs exhibit a coordinated Mk transcription profile and efficiently upregulate Mk protein synthesis upon inflammation. The hypothesis that commitment of HSCs to SL-MkPs is associated with a switch from a stochastic toward a coordinated Mk transcription program was further supported by a significant drop in the Fano factor, an indicator for a system's stochasticity and transcriptional noise (Figure S5A) (Munsky et al., 2012; Ozbudak et al., 2002).

Profiling of transcription factors (TFs) in single HSCs revealed that expression of many known Mk TFs correlated with Mk-commitment (e.g., highest expression in classical MkPs and SL-MkPs) and expression of Mk lineage transcripts (Figures S5B–S5D). This suggests that Mk transcriptional priming and Mk lineage commitment of SL-MkPs are established by transcriptional regulators during homeostasis, while inflammation drives a post-transcriptional Mk protein synthesis from these pre-existing transcripts.

To investigate how closely related multipotent HSCs and SL-MkPs are, we performed global gene expression analysis of single HSCs and $Lin^{-}cKit^{+}CD150^{-}$ progenitors using a customized single-cell RNA-sequencing (seq) approach. In accordance with our single-cell qPCR data, Mk transcripts were significantly enriched among the most variably expressed genes and Mk lineage priming differed dramatically between individual HSCs, whereas progenitors consistently showed little or no Mk lineage transcript expression (Figures S5E, 5E, and 5F). To determine whether the transcriptome of HSCs with high Mk lineage priming differs from HSCs with low Mk lineage priming, we performed PCA of HSCs and color-coded each cell with a calculated Mk Gene Set Enrichment Analysis (GSEA)-score reflecting the degree of Mk lineage priming (Figure 5G). Importantly, genome-wide expression profiles did not correlate with the degree of Mk-lineage priming, suggesting that Mk-primed HSCs (e.g., SL-MkPs) and HSCs with low Mk lineage priming are highly related cell types. Together, these data suggest that multipotent

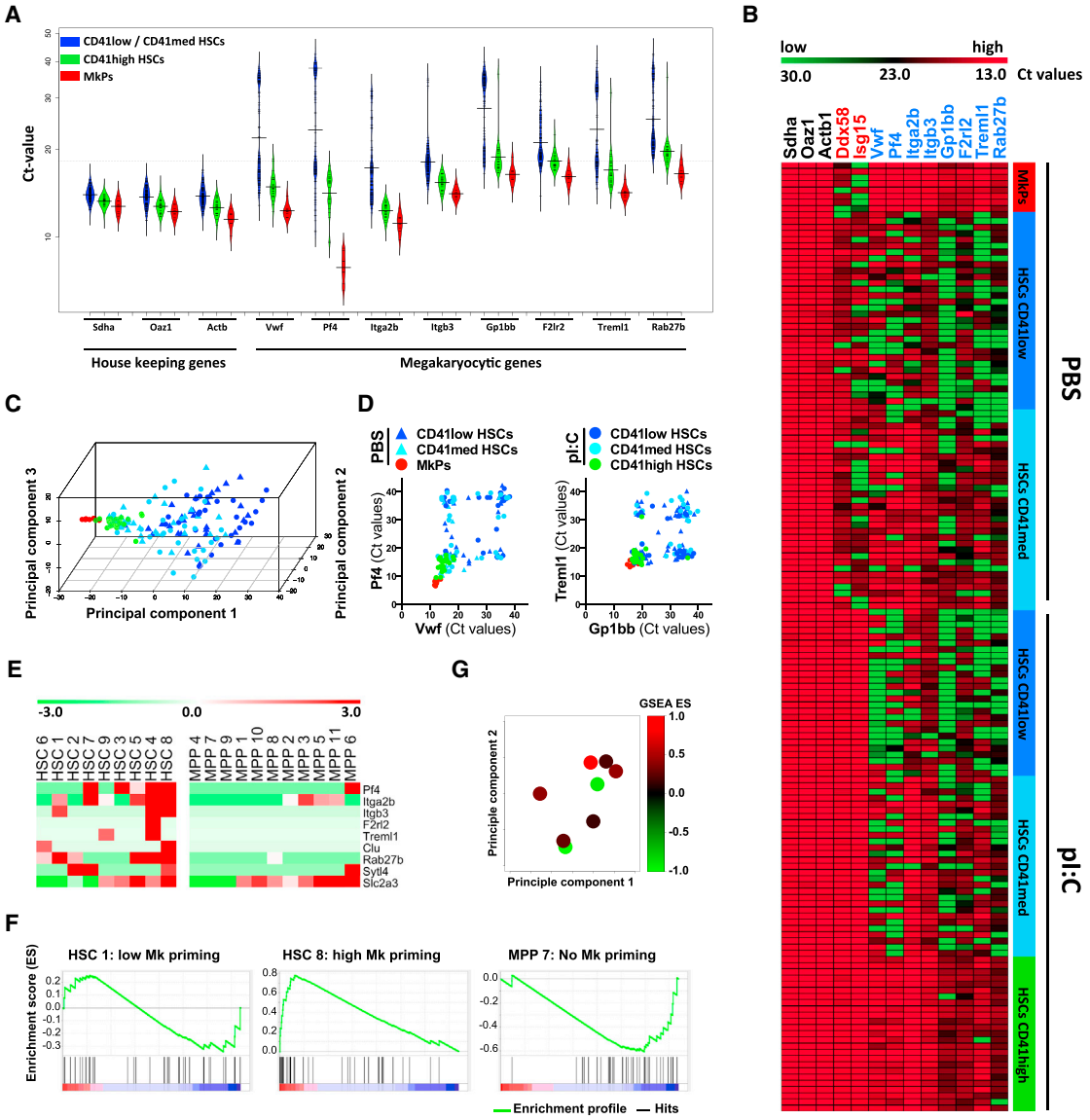

Figure 5. HSCs Switch from a Stochastic to a Coordinated Mk Transcript Expression Program upon Commitment from Multipotency toward the Mk Lineage

(A–D) Single-cell qPCR of LT-HSC CD41 sub-populations. (A) Bean plot representation of Mk transcripts of MkPs and LT-HSCs with homeostatic CD41 expression (CD41low and CD41med) of PBS or pI:C treated mice or with elevated CD41 levels (CD41high and SL-MkPs) of pI:C treated mice. (B) Heatmap indicating transcript expression of housekeeping genes (Sdha, Oaz1, and Actb), IFN response genes (Ddx58 and Isg15), and Mk genes (others). (C) PCA of CD41 sub-populations of LT-HSCs based on their Mk transcript expression values. The labels are as indicated in (D). (D) Transcript expression of Vwf versus Pf4 (left) and Treml1 versus Gp1bb (right). The expression values are presented as Ct-values.

(E–G) Single-cell RNA-seq of Lin$^-$cKit$^+$CD150$^+$CD48$^-$ HSCs and Lin$^-$cKit$^+$C150$^-$ progenitors. (E) Heatmap of HSCs and progenitors showing expression of Mk and platelet cluster genes in individual cells that were detected with at least 50 reads per cell on average and were significantly differentially expressed. (F) GSEA of Mk cluster genes in single HSCs and progenitors. The exemplary GSEA profiles are shown. (G) PCA of HSCs based on their overall transcriptome. The individual cells are color-coded according to their Mk GSEA enrichment score (ES). See also Figure S5.

HSCs and SL-MkPs exhibit a related overall transcriptome, however, commitment from multipotent HSCs to SL-MkPs is associated with a switch from a stochastic to a coordinated Mk transcription program. High transcriptional Mk priming provides SL-MkPs with the appropriate transcripts to mount an efficient post-transcriptional Mk protein synthesis program upon inflammatory signaling.

SL-MkPs Represent an Mk-Committed Sub-Population of VWF$^+$ HSCs

VWF$^+$ HSCs represent a multipotent, but Mk-biased, sub-population of HSCs that has been defined by high transcriptional expression of the *Vwf* gene (Sanjuan-Pla et al., 2013). To directly compare SL-MkPs with VWF$^+$ HSCs, we separated LT-HSCs depending on their *Vwf* transcriptional activity (Figure S5F).

VWF$^+$ HSCs showed an enriched Mk transcriptional priming if compared to VWF$^-$ HSCs (Figure S5F) (Sanjuan-Pla et al., 2013). However, only a small sub-fraction of VWF$^+$ HSCs showed expression of all Mk transcripts. In contrast, SL-MkPs uniformly showed high expression of all Mk genes including *Vwf,* correlating with their commitment to the Mk-lineage. Thus, SL-MkPs represent an Mk-committed sub-population of VWF$^+$ HSCs. These data are consistent with a model where VWF$^+$ HSCs preferentially give rise to SL-MkPs, thereby establishing the Mk-bias of multipotent VWF$^+$ HSCs.

The Most Potent and Primitive SL-MkPs Reside in a Dormant State and Are Efficiently Activated upon Inflammation

The most potent HSCs are maintained in a long-term quiescent (dormant) state where they serve as a reserve pool for conditions of acute stress (Wilson et al., 2008). Long-term quiescent, label-retaining cells (LRCs) can be identified in the HSC compartment using doxycyclin (dox) treatment of SCL-tTA:H2B-GFP mice (Wilson et al., 2008). Whether dormant lineage-restricted progenitors exist in the phenotypic HSC compartment is unknown. Interestingly, an inflammation-mediated increase in Mk protein expression, cell size, and granularity could be observed both in non-LRC LT-HSCs and in dormant LRC LT-HSCs, suggesting that SL-MkPs also exist in a dormant state (Figures 6A–6C, S6A, and S6B). Accordingly, single-cell ex vivo lineage tracking showed that SL-MkPs exclusively generating mature Mks could be found both in the non-LRC fraction and in the dormant LRC fraction of the LT-HSC compartment. Interestingly, dormant SL-MkPs formed larger Mk-colonies and required a longer time to generate the first mature Mks when compared to their non-LRC counterparts (Figure 6D). This suggests that the most primitive and most potent SL-MkPs reside in a dormant state and, hence, do not contribute to steady-state megakaryopoiesis.

To investigate whether quiescent SL-MkPs are activated upon inflammation, we measured cell cycle activity in HSC CD41 sub-populations. Ki67-Hoechst and BrdU incorporation assays revealed a rapid and efficient cell cycle entry of SL-MkPs that increased Mk protein levels 16 hr post pI:C treatment, whereas the remaining HSC pool was activated at later time points (Figures 6E–6G and S6E). Accordingly, inflammation triggered by LPS or TNFα injection resulted in a similar cell cycle induction of these SL-MkPs that increased Mk protein levels (Figure S6C), demonstrating that distinct inflammatory signals efficiently activate quiescent SL-MkPs.

FoxO3a is a key TF that instructs transcription of the cell cycle inhibitors p27, p57, p107, and p130, thereby maintaining HSCs in a quiescent state (Miyamoto et al., 2007; Tothova and Gilliland, 2007). Cell cycle entry of HSCs is frequently associated with FoxO3a phosphorylation and subsequent exclusion from the nucleus (Tothova and Gilliland, 2007). In phenotypic HSCs from control mice and HSCs from pI:C treated mice with homeostatic CD41 expression, FoxO3a was localized mainly to the nucleus. In contrast, in CD41*high* HSCs (i.e., SL-MkPs) from pI:C treated mice, FoxO3a was frequently redirected to the cytoplasm, suggesting that FoxO3a inactivation is associated with inflammation-induced cell cycle entry of SL-MkPs (Figures 6H and S6D). In accordance, a significant decrease in expression of FoxO3a targets p27, p57, p107, and p130 was specifically observed in SL-MkPs that increased Mk proteins, whereas p19, which is not a FoxO3a target, remained unchanged (Figure 6I). Together, these data suggest that acute inflammation triggers FoxO3a inactivation and efficient cell cycle activation of quiescent SL-MkPs.

Repeated Cycles of Type-I IFN Mediated Inflammation Trigger the Exhaustion of SL-MkPs and Other Megakaryocytic Progenitors

We have shown that a single induction of inflammation drives maturation of SL-MkPs and MkPs. Accordingly, repeated cycles of inflammation over a long time period would be anticipated to result in an exhaustion of these cell types. To investigate this hypothesis, mice were treated with pI:C every 3 days for a time period of 30 days (ten doses) (Figure 7A). While a single pI:C dose resulted in an augmented Mk protein production in HSCs and MkPs, as well as in an increase in mature polyploid Mks as described above, inflammation-mediated Mk protein production and the number of MkPs and mature polyploid Mks was significantly reduced upon repeated doses of pI:C (Figures 7B–7D). Regeneration from platelet consumption after single pI:C treatment was accomplished within 7 days, whereas after ten doses, the hematopoietic system required longer to rebuild the platelet pool, reflecting the reduction in MkPs and SL-MkPs (Figure 7E). These data indicate that repeated cycles of pI:C-mediated inflammation can result in a transient exhaustion of MkPs and SL-MkPs due to a constant drive toward maturation, which prevents an efficient platelet recovery after inflammation-mediated platelet loss.

DISCUSSION

During infection, platelets actively counteract infectious agents by releasing immunomodulatory agents and interacting with neutrophils to trap pathogens (Jenne et al., 2013; Yeaman, 2014), thereby, being rapidly consumed. Since low platelet levels during inflammation are associated with loss of vascular integrity and septic shock (Goerge et al., 2008; Xiang et al., 2013), a rapid recovery of platelet levels is of fundamental importance. We show that inflammatory signaling instructs a rapid Mk maturation program at distinct levels of megakaryopoiesis to regenerate the lost platelet pool. While MkPs are efficiently driven into endomitosis, leading to a strong increase in mature Mks, a small pool of potent Mk-committed progenitors (SL-MkPs) within the phenotypic HSC compartment replaces the lost MkPs. Even though SL-MkPs and classical MkPs appear to be closely related in their lineage potential and their coordinated Mk transcription profile, SL-MkPs share many features with HSCs which set them apart from MkPs. Similar to HSCs, and in contrast to MkPs, SL-MkPs are small in cell size, suppress Mk protein production, and are mainly quiescent. Due to their quiescent, partly dormant nature, SL-MkPs contribute little to steady-state megakaryopoiesis, but serve as an emergency pool for inflammatory insult.

As a result of their quiescence and the suppression of Mk protein production, SL-MkPs are maintained in a metabolically inactive, but primed, state, allowing them to be readily activated. Inflammatory signaling triggers FoxO3a inactivation, resulting in cell cycle activation of quiescent SL-MkP. Moreover, inflammation-mediated maturation of SL-MkPs is associated with mTOR

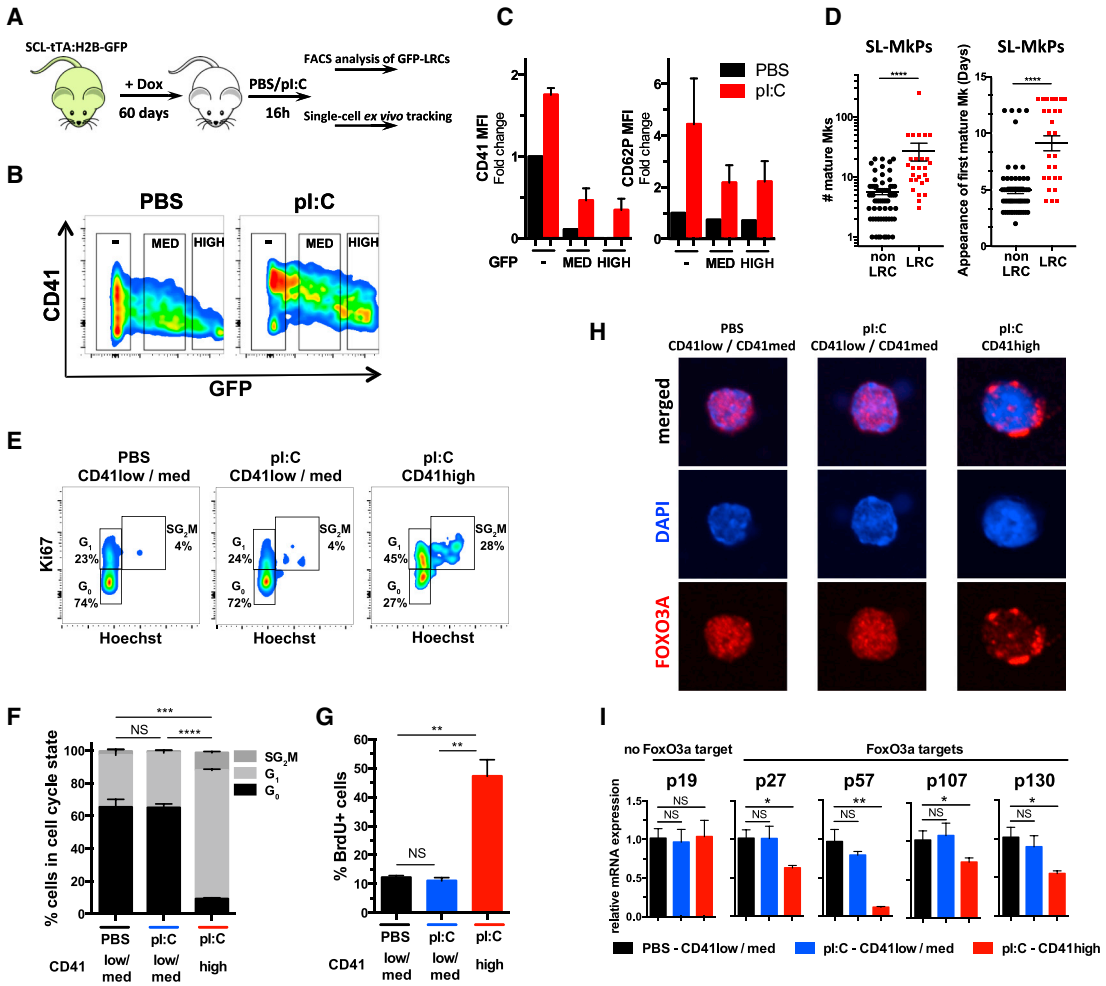

Figure 6. The Most Potent and Primitive SL-MkPs Reside in a Dormant State and Are Efficiently Activated upon Inflammation

(A–D) LRC assays. The dormant HSCs were labeled by administering dox to SCL-tTA:H2B-GFP mice for 60 days, followed by PBS or pI:C treatment. Subsequently, Mk protein expression was measured in HSCs (B and C) or mice were subjected to single-cell ex vivo lineage tracking (D). (A) Illustration of experimental approach. (B) Representative FACS plots after 60 days of chase, followed by PBS or pI:C treatment, in LT-HSCs. (C) Quantification of Mk protein expression. (D) Mk only colonies formed from GFP^{low} non-LRC-HSCs and GFP^{high} LRC-HSCs. The number of mature Mks formed at day 14 of culture (left). The time until first mature Mk cell appears in the culture (right).

(E) Representative FACS plots of Ki67-Hoechst cell-cycle stainings of HSC CD41 sub-populations.

(F) Quantification of Ki67-Hoechst cell cycle measurements.

(G) Cell cycle analysis of HSC CD41 sub-populations measured by BrdU incorporation.

(H) Representative confocal microscopy images of indicated CD41 LT-HSCs sub-populations, stained for FoxO3a (red) and DAPI (blue).

(I) Transcript levels of cell cycle inhibitors measured by qPCR in CD41 sub-populations of LT-HSCs.

In (C), (D), (F), (G), and (I), data are presented as mean ± SEM with n ≥ 3. The significance was determined using the Mann-Whitney-Wilcoxon test (D) or an unpaired, two-tailed student's t test (F, G, and I) (*p ≤ 0.05, **p ≤ 0.01, ***p ≤ 0.001, ****p ≤ 0.0001, and non-significant: NS). See also Figure S6.

and STAT1 dependent increase in cell size, enhanced Mk protein production, and appearance of alpha granular precursors. In line with our findings, both mTOR and STAT1 signaling have been previously implicated in megakaryopoiesis (Huang et al., 2007; Raslova et al., 2006).

During homeostasis, post-transcriptional regulation of gene expression is a rare event in HSCs and changes in protein and mRNA levels are highly correlated during commitment (Cabezas-Wallscheid et al., 2014). In contrast to homeostasis, our findings reveal the presence of significant post-transcriptional regulation in response to acute inflammation. Our data suggest that Mk transcripts are expressed, but that translation is repressed during homeostasis, resulting in low Mk protein production, whereas inflammatory signaling drives efficient translation of these transcripts, revealing an important role for Mk lineage priming during emergency megakaryopoiesis. This model is supported by recent findings demonstrating that HSCs suppress protein synthesis during homeostasis (Signer et al., 2014). Our single-cell gene expression data provide novel insights into the basis of Mk lineage priming and suggest that multipotent HSCs and SL-MkPs exhibit highly related transcriptomes, but switch from a stochastic to a coordinated Mk

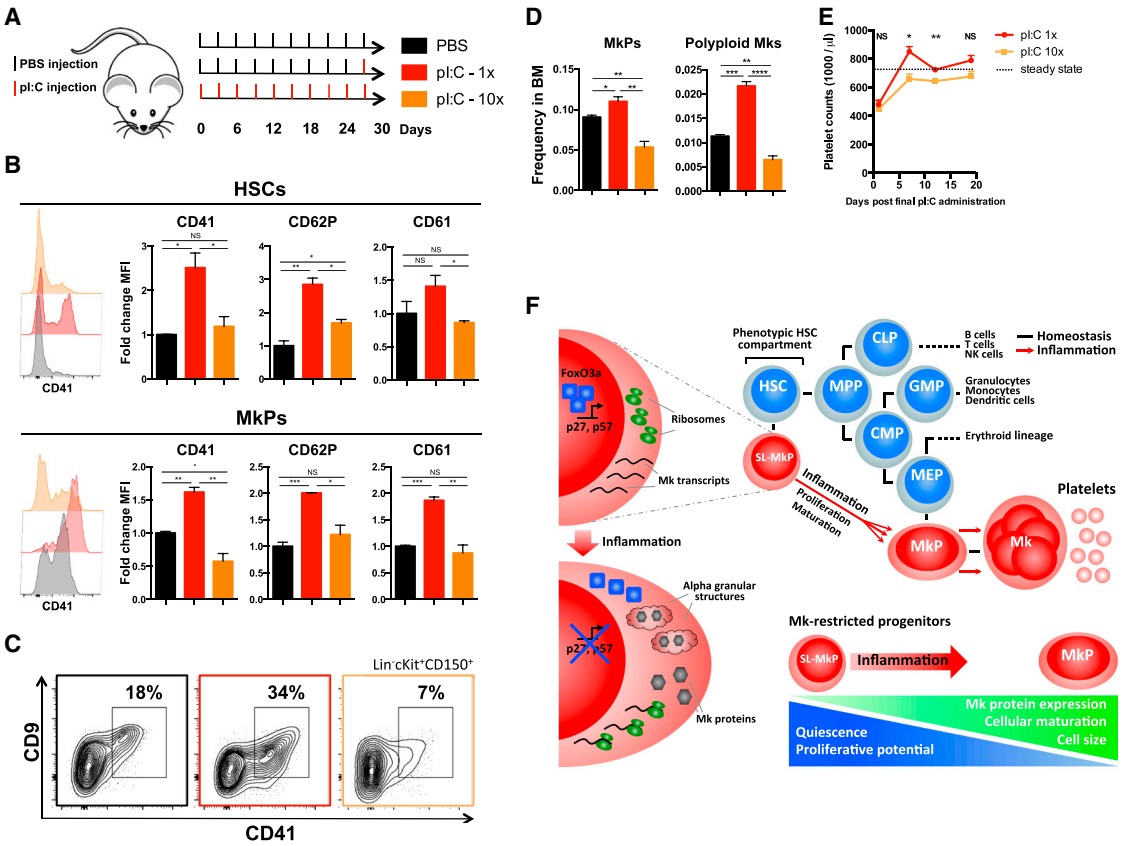

Figure 7. Chronic Inflammation Triggers Exhaustion of SL-MkPs and Other MkPs

(A–E) Mice were treated every third day for a 30 day period with pI:C. At 16 hr after the final administration, HSCs and MkPs were FACS-analyzed (B–D) or platelet recovery was investigated (E). For control purposes, mice were treated with PBS in the same schedule or with PBS and single final pI:C dose. (A) Illustration of experimental approach. (B) Flow cytometric analysis of Mk protein expression in HSCs or MkPs. (C) Representative FACS plot of Lin$^-$cKit$^+$CD150$^+$ bone marrow cells and CD41 and CD9 expression. (D) Quantification of MkPs and polyploid Mks. (E) Platelet recovery after chronic and acute inflammation.

(F) Model.

In (B), (D), and (E), data are presented as mean ± SEM with n ≥ 3. The significance was determined using an unpaired, two-tailed student's t test (*p ≤ 0.05, **p ≤ 0.01, ***p ≤ 0.001, ****p ≤ 0.0001, and non-significant: NS).

transcription program upon commitment from multipotent HSCs toward the Mk lineage.

Recent reports suggested the existence of Mk-biased, but multipotent, HSCs (Sanjuan-Pla et al., 2013; Shin et al., 2014). SL-MkPs represent a sub-population of VWF$^+$ HSCs, which in contrast to the VWF$^+$ HSCs are homogenously restricted to the Mk lineage reflected in their coordinated Mk transcription profile. A preferential commitment of Mk-biased HSCs to SL-MkPs could explain their intrinsic Mk lineage bias. In accordance with our data, single-cell transplantations of phenotypic HSCs revealed the existence of Mk-restricted progenitors with high self-renewal activity probably directly originating from HSCs (Yamamoto et al., 2013), likely representing the cells defined by our study as SL-MkPs.

In this study, we make use of CD41 expression to discriminate SL-MkPs during inflammation. During homeostasis, CD41 is expressed at low levels by HSCs and other myeloid progenitors (Gekas and Graf, 2013; Yamamoto et al., 2013). Due to an intrinsic repression of Mk protein synthesis, SL-MkPs express CD41 to similar levels as HSCs during homeostasis, but efficiently induce CD41 expression upon inflammatory signaling. This suggests that high expression of CD41 is a marker for Mk commitment, while CD41 has broader roles in hematopoiesis as highlighted by the fact that CD41$^{-/-}$ mice display multilineage hematopoietic defects (Gekas and Graf, 2013). A recent study reported an increased CD41 expression in HSCs upon aging (Gekas and Graf, 2013). Accordingly, also the expression of other Mk proteins such as CD62P and Vwf increased in the phenotypic HSC compartment upon aging, and treatment of aged mice with pI:C triggered Mk protein synthesis to even higher levels (data not shown). These data are in line with a potential expansion or enhanced maturation of SL-MkPs during aging.

While acute inflammatory signaling drives rapid maturation of MkPs, resulting in increased platelet production, repeated cycles of type-I IFN-mediated inflammation can trigger a constant push of maturation and thus a partial exhaustion of MkPs. These findings reveal that depending on the context and timing, the same inflammatory stimuli can be associated with opposing effects on megakaryopoiesis. This sheds light on the question of why some inflammatory states and diseases are associated with thrombocytosis, whereas others provoke thrombocytopenia

(Cole et al., 1998; Kawamoto, 2003; Martin and Shuman, 1998; Rajan et al., 2005).

EXPERIMENTAL PROCEDURES

In Vivo Treatments

To induce an inflammation, mice were injected intraperitoneal with a single dose of 5 mg/kg pI:C (Invitrogen), 0.25 mg/kg LPS (Sigma), or 0.75 mg/kg recombinant TNFα (PeproTech). Alternatively, mice were treated every third day for 30 days with 5 mg/kg pI:C. Platelet depletion was performed by intravenous injection of 2 mg/kg rat monoclonal antibody directed against mouse GPIb (Emfret Analytics). For transient mTOR blockage, mice were pretreated with 1.5 mg/kg rapamycin 2 hr prior to pI:C treatment.

Transplantation Experiments

For transplantation experiments, $Lin^-cKit^+CD150^+CD48^-CD34^-CD41^{low/med/high}$ HSC populations were FACS-sorted from ACTB-dtTomato mice. 40 HSCs together with 2×10^5 supportive $CD45.2^+$ WT BM were transplanted intrafemorally into lethally irradiated (2 × 500 radiation absorbed dose [rad]) $CD45.2^+$ recipient mice. Peripheral blood was collected at indicated time points and analyzed for $tomato^+$ cells by flow cytometry.

Quantitative Proteomics

Proteomic analysis was performed as described previously (Cabezas-Wallscheid et al., 2014), with minor differences.

H2B-GFP Label-Retention Assays

In vivo label-retention assays using SCL-tTA:H2B-GFP mice were performed as previously described (Wilson et al., 2008). SCL-tTA:H2B-GFP mice were maintained on water containing 2 mg/ml doxycyline hydrate (Sigma) in 5% glucose for a 60 day chase period.

Single-Cell qPCR and Single-Cell RNA-Seq

Single cells were directly sorted into PCR-tubes loaded with lysis buffer using a BD FACSAria II (BD Bioscience) under the single-cell mode. Single-cell qPCR was essentially performed as previously described (Guo et al., 2013), with minor differences. Single-cell RNA-seq was performed according to a modified version of the QUARTZ-Seq protocol (Sasagawa et al., 2013).

Single-Cell Ex Vivo Lineage Tracking

Single-cell ex vivo lineage tracking was performed according to a modified version of the approach described by Eilken et al. (2009).

Electron Microscopy

Transmission electron microscopy was performed as described previously (Platani et al., 2009), with minor differences.

ACCESSION NUMBERS

The proteomics data have been deposited to ProteomeXchange Consortium and are accessible at http://www.ebi.ac.uk/pride with the dataset identifier: PXD001500. The single-cell RNA-seq data can be accessed under Gene Expression Omnibus under accession number GSE64002.

SUPPLEMENTAL INFORMATION

Supplemental Information includes Supplemental Experimental Procedures, six figures, and one table and can be found with this article online at http://dx.doi.org/10.1016/j.stem.2015.07.007.

AUTHOR CONTRIBUTIONS

J.H., D.K., S.H., S.W., A.T., J.K., and M.A.G.E. designed, performed, and/or analyzed proteomics experiments. D.K., J.H., R.S.-M., A.T., and J.K. designed, performed, and/or analyzed electron microscopy experiments. L.V., S.H., K.H., M.A.G.E., and L.M.S. designed, performed, and/or analyzed single-cell RNA-seq experiments. D.L., S.H., M.A.G.E., and T.S. designed, performed, and/or analyzed single-cell ex vivo tracking experiments. S.H., H.U., S.W., A.M.P., A.S., S.B., A.K., M.D.M., and M.A.G.E. designed, performed, and/or analyzed all other in vivo and ex vivo experiments. S.H., J.H., D.K., D.L., L.V., A.M.P., M.D.M., L.M.S., T.S., A.T., J.K., and M.A.G.E. wrote the manuscript.

ACKNOWLEDGMENTS

We would like to thank A. Atzberger and S. Schmitt from the Deutsches Krebsforschungszentrum (DKFZ) Flow Cytometry Facility; D. Krunic from the DKFZ Imaging Core Facility; J. Kirkpatrick, S. Leicht, and K. Dzeyk from the EMBL Proteomics Core Facility; C. Funaya, C. Antony, and Y. Schwab from the EMBL Electron Microscopy Core Facility; members from the EMBL Genomics Core Facility; and the DKFZ Animal Laboratory Services for assistance and their expertise. This work was supported by the BioRN Leading-Edge Cluster "Cell-Based and Molecular Medicine" funded by the German Federal Ministry of Education and Research, the Dietmar Hopp Foundation, and the SFB873 and FOR2033 NicHem, both funded by the Deutsche Forschungsgemeinschaft (DFG).

Received: December 12, 2014
Revised: May 29, 2015
Accepted: July 13, 2015
Published: August 20, 2015

REFERENCES

Baldridge, M.T., King, K.Y., Boles, N.C., Weksberg, D.C., and Goodell, M.A. (2010). Quiescent haematopoietic stem cells are activated by IFN-gamma in response to chronic infection. Nature *465*, 793–797.

Browne, E.P., Wing, B., Coleman, D., and Shenk, T. (2001). Altered cellular mRNA levels in human cytomegalovirus-infected fibroblasts: viral block to the accumulation of antiviral mRNAs. J. Virol. *75*, 12319–12330.

Cabezas-Wallscheid, N., Klimmeck, D., Hansson, J., Lipka, D.B., Reyes, A., Wang, Q., Weichenhan, D., Lier, A., von Paleske, L., Renders, S., et al. (2014). Identification of regulatory networks in HSCs and their immediate progeny via integrated proteome, transcriptome, and DNA methylome analysis. Cell Stem Cell *15*, 507–522.

Cole, J.L., Marzec, U.M., Gunthel, C.J., Karpatkin, S., Worford, L., Sundell, I.B., Lennox, J.L., Nichol, J.L., and Harker, L.A. (1998). Ineffective platelet production in thrombocytopenic human immunodeficiency virus-infected patients. Blood *91*, 3239–3246.

Dorrello, N.V., Peschiaroli, A., Guardavaccaro, D., Colburn, N.H., Sherman, N.E., and Pagano, M. (2006). S6K1- and betaTRCP-mediated degradation of PDCD4 promotes protein translation and cell growth. Science *314*, 467–471.

Eilken, H.M., Nishikawa, S., and Schroeder, T. (2009). Continuous single-cell imaging of blood generation from haemogenic endothelium. Nature *457*, 896–900.

Essers, M.A., Offner, S., Blanco-Bose, W.E., Waibler, Z., Kalinke, U., Duchosal, M.A., and Trumpp, A. (2009). IFNalpha activates dormant haematopoietic stem cells in vivo. Nature *458*, 904–908.

Gekas, C., and Graf, T. (2013). CD41 expression marks myeloid-biased adult hematopoietic stem cells and increases with age. Blood *121*, 4463–4472.

Goerge, T., Ho-Tin-Noe, B., Carbo, C., Benarafa, C., Remold-O'Donnell, E., Zhao, B.Q., Cifuni, S.M., and Wagner, D.D. (2008). Inflammation induces hemorrhage in thrombocytopenia. Blood *111*, 4958–4964.

Guo, G., Luc, S., Marco, E., Lin, T.W., Peng, C., Kerenyi, M.A., Beyaz, S., Kim, W., Xu, J., Das, P.P., et al. (2013). Mapping cellular hierarchy by single-cell analysis of the cell surface repertoire. Cell Stem Cell *13*, 492–505.

Heijnen, H.F., Debili, N., Vainchencker, W., Breton-Gorius, J., Geuze, H.J., and Sixma, J.J. (1998). Multivesicular bodies are an intermediate stage in the formation of platelet alpha-granules. Blood *91*, 2313–2325.

Huang, Z., Richmond, T.D., Muntean, A.G., Barber, D.L., Weiss, M.J., and Crispino, J.D. (2007). STAT1 promotes megakaryopoiesis downstream of GATA-1 in mice. J. Clin. Invest. *117*, 3890–3899.

Ingolia, N.T., Brar, G.A., Rouskin, S., McGeachy, A.M., and Weissman, J.S. (2012). The ribosome profiling strategy for monitoring translation in vivo by deep sequencing of ribosome-protected mRNA fragments. Nat. Protoc. *7*, 1534–1550.

Jenne, C.N., Wong, C.H., Zemp, F.J., McDonald, B., Rahman, M.M., Forsyth, P.A., McFadden, G., and Kubes, P. (2013). Neutrophils recruited to sites of infection protect from virus challenge by releasing neutrophil extracellular traps. Cell Host Microbe *13*, 169–180.

Kawamoto, T. (2003). Use of a new adhesive film for the preparation of multi-purpose fresh-frozen sections from hard tissues, whole-animals, insects and plants. Arch. Histol. Cytol. *66*, 123–143.

Kruiswijk, F., Yuniati, L., Magliozzi, R., Low, T.Y., Lim, R., Bolder, R., Mohammed, S., Proud, C.G., Heck, A.J., Pagano, M., and Guardavaccaro, D. (2012). Coupled activation and degradation of eEF2K regulates protein synthesis in response to genotoxic stress. Sci. Signal. *5*, ra40.

Liu, J., Xu, Y., Stoleru, D., and Salic, A. (2012). Imaging protein synthesis in cells and tissues with an alkyne analog of puromycin. Proc. Natl. Acad. Sci. USA *109*, 413–418.

Machlus, K.R., and Italiano, J.E., Jr. (2013). The incredible journey: From megakaryocyte development to platelet formation. J. Cell Biol. *201*, 785–796.

Månsson, R., Hultquist, A., Luc, S., Yang, L., Anderson, K., Kharazi, S., Al-Hashmi, S., Liuba, K., Thorén, L., Adolfsson, J., et al. (2007). Molecular evidence for hierarchical transcriptional lineage priming in fetal and adult stem cells and multipotent progenitors. Immunity *26*, 407–419.

Martin, T.G., and Shuman, M.A. (1998). Interferon-induced thrombocytopenia: is it time for thrombopoietin. Hepatology *28*, 1430–1432.

Miyamoto, K., Araki, K.Y., Naka, K., Arai, F., Takubo, K., Yamazaki, S., Matsuoka, S., Miyamoto, T., Ito, K., Ohmura, M., et al. (2007). Foxo3a is essential for maintenance of the hematopoietic stem cell pool. Cell Stem Cell *1*, 101–112.

Munsky, B., Neuert, G., and van Oudenaarden, A. (2012). Using gene expression noise to understand gene regulation. Science *336*, 183–187.

Orkin, S.H., and Zon, L.I. (2008). Hematopoiesis: an evolving paradigm for stem cell biology. Cell *132*, 631–644.

Ozbudak, E.M., Thattai, M., Kurtser, I., Grossman, A.D., and van Oudenaarden, A. (2002). Regulation of noise in the expression of a single gene. Nat. Genet. *31*, 69–73.

Platani, M., Santarella-Mellwig, R., Posch, M., Walczak, R., Swedlow, J.R., and Mattaj, I.W. (2009). The Nup107-160 nucleoporin complex promotes mitotic events via control of the localization state of the chromosome passenger complex. Mol. Biol. Cell *20*, 5260–5275.

Platanias, L.C. (2005). Mechanisms of type-I- and type-II-interferon-mediated signalling. Nat. Rev. Immunol. *5*, 375–386.

Rajan, S.K., Espina, B.M., and Liebman, H.A. (2005). Hepatitis C virus-related thrombocytopenia: clinical and laboratory characteristics compared with chronic immune thrombocytopenic purpura. Br. J. Haematol. *129*, 818–824.

Raslova, H., Baccini, V., Loussaief, L., Comba, B., Larghero, J., Debili, N., and Vainchenker, W. (2006). Mammalian target of rapamycin (mTOR) regulates both proliferation of megakaryocyte progenitors and late stages of megakaryocyte differentiation. Blood *107*, 2303–2310.

Sanjuan-Pla, A., Macaulay, I.C., Jensen, C.T., Woll, P.S., Luis, T.C., Mead, A., Moore, S., Carella, C., Matsuoka, S., Bouriez Jones, T., et al. (2013). Platelet-biased stem cells reside at the apex of the haematopoietic stem-cell hierarchy. Nature *502*, 232–236.

Sasagawa, Y., Nikaido, I., Hayashi, T., Danno, H., Uno, K.D., Imai, T., and Ueda, H.R. (2013). Quartz-Seq: a highly reproducible and sensitive single-cell RNA sequencing method, reveals non-genetic gene-expression heterogeneity. Genome Biol. *14*, R31.

Semple, J.W., Italiano, J.E., Jr., and Freedman, J. (2011). Platelets and the immune continuum. Nat. Rev. Immunol. *11*, 264–274.

Shin, J.Y., Hu, W., Naramura, M., and Park, C.Y. (2014). High c-Kit expression identifies hematopoietic stem cells with impaired self-renewal and megakaryocytic bias. J. Exp. Med. *211*, 217–231.

Signer, R.A., Magee, J.A., Salic, A., and Morrison, S.J. (2014). Haematopoietic stem cells require a highly regulated protein synthesis rate. Nature *509*, 49–54.

Stohlawetz, P., Folman, C.C., von dem Borne, A.E., Pernerstorfer, T., Eichler, H.G., Panzer, S., and Jilma, B. (1999). Effects of endotoxemia on thrombopoiesis in men. Thromb. Haemost. *81*, 613–617.

Tacchini-Cottier, F., Vesin, C., Redard, M., Buurman, W., and Piguet, P.F. (1998). Role of TNFR1 and TNFR2 in TNF-induced platelet consumption in mice. J. Immunol. *160*, 6182–6186.

Tothova, Z., and Gilliland, D.G. (2007). FoxO transcription factors and stem cell homeostasis: insights from the hematopoietic system. Cell Stem Cell *1*, 140–152.

Wilson, A., Laurenti, E., Oser, G., van der Wath, R.C., Blanco-Bose, W., Jaworski, M., Offner, S., Dunant, C.F., Eshkind, L., Bockamp, E., et al. (2008). Hematopoietic stem cells reversibly switch from dormancy to self-renewal during homeostasis and repair. Cell *135*, 1118–1129.

Xiang, B., Zhang, G., Guo, L., Li, X.A., Morris, A.J., Daugherty, A., Whiteheart, S.W., Smyth, S.S., and Li, Z. (2013). Platelets protect from septic shock by inhibiting macrophage-dependent inflammation via the cyclooxygenase 1 signalling pathway. Nat. Commun. *4*, 2657.

Yamamoto, R., Morita, Y., Ooehara, J., Hamanaka, S., Onodera, M., Rudolph, K.L., Ema, H., and Nakauchi, H. (2013). Clonal analysis unveils self-renewing lineage-restricted progenitors generated directly from hematopoietic stem cells. Cell *154*, 1112–1126.

Yeaman, M.R. (2014). Platelets: at the nexus of antimicrobial defence. Nat. Rev. Microbiol. *12*, 426–437.

Cell Stem Cell

Supplemental Information

Inflammation-Induced Emergency Megakaryopoiesis Driven by Hematopoietic Stem Cell-like Megakaryocyte Progenitors

Simon Haas, Jenny Hansson, Daniel Klimmeck, Dirk Loeffler, Lars Velten, Hannah Uckelmann, Stephan Wurzer, Áine M. Prendergast, Alexandra Schnell, Klaus Hexel, Rachel Santarella-Mellwig, Sandra Blaszkiewicz, Andrea Kuck, Hartmut Geiger, Michael D. Milsom, Lars M. Steinmetz, Timm Schroeder, Andreas Trumpp, Jeroen Krijgsveld, and Marieke A.G. Essers

SUPPLEMENTAL FIGURE LEGENDS

Figure S1, related to Figure 1. Inflammation Drives Megakaryocytic Protein Production in HSCs.

(A) FACS gating scheme for immunophenotypic discrimination of HSCs ($Lin^-cKit^+CD150^+CD48^-$) and LT-HSCs ($Lin^-cKit^+CD150^+CD48^-CD34^-$).

(B) Lineage-negative cells (left panel), $Lin^-cKit^+CD150^+CD48^-$ HSCs (middle panel), and $Lin^-cKit^+CD150^+CD48^-CD34^-$ LT-HSCs (right panel) were investigated for their Sca-1, EPCR, ESAM and Flt3 expression. Phenotypic HSCs and LT-HSCs as defined by our gating strategy are homogeneously positive for the other HSC markers Sca-1, EPCR and ESAM, and negative for the negative HSC marker Flt3 and thus correspond to $Lin^-cKit^+CD150^+CD48^-Sca\text{-}1^+EPCR^+ESAM^+Flt3^-(CD34^-)$ cells.

(C) Phenotypic committed progenitors as defined by our gating strategy are negative for Sca-1. Megakaryocyte Progenitors: MkPs; Megakaryocyte-Erythroid Progenitors: MEPs; Granulocyte-Monocyte Progenitors: GMPs; CFU-E; Colony Forming Unit Erythroid. See supplemental experimental procedures for gating strategies of committed progenitors.

(D-F) Mass spectrometry-based quantitative proteome analysis of HSCs and progenitors from PBS and pI:C treated mice.

(D) Top 10 enriched Gene Ontology (GO) cellular processes of up-regulated proteins upon pI:C treatment in WT mice. Dashed line shows limit of statistical significance (p=0.05). Highly similar terms were removed to show diverse processes.

(E) Protein interaction networks of proteins with differential expression in at least one of the WT or $IFNAR^{-/-}$ HSC proteomics analyses, mapped onto the data of each analysis.

(F) Scatter plot of adjusted p-values of protein changes in HSCs and progenitors upon pI:C treatment. Proteins of the interferon response cluster and Mk and platelet cluster are highlighted in red and blue respectively.

(G) Recombinant IFNα drives Mk protein synthesis in phenotypic HSCs. HSCs from PBS, IFNα and pI:C treated WT mice were analyzed for CD41 and CD62P protein expression by flow cytometry (16h after injection). Data are presented as fold change in MFI, mean ±SEM are indicated, $n \geq 3$.

(H) WT:IFNAR$^{-/-}$ chimeras. Chimeras were created by transplanting WT, IFNAR$^{-/-}$ or 50% WT + 50% IFNAR$^{-/-}$ bone marrow into lethally irradiated WT and / or IFNAR$^{-/-}$ recipients. 8-10 weeks after transplantation, chimeras were treated with PBS or pI:C and HSCs were analyzed for Mk protein expression 16h after treatment.

(I) IFN-STAT1 signaling is involved in Mk protein up-regulation in HSCs and MkPs. HSCs and MkPs from PBS and pI:C treated WT, IFNAR$^{-/-}$ and STAT1$^{-/-}$ mice were analyzed for CD41 and CD62P protein expression by flow cytometry (16h after injection). Data are presented as fold change in MFI, mean ±SEM are indicated, $n \geq 3$.

(J) Rapamycin pretreatment of mice partly blocks pI:C-mediated CD41 protein up-regulation in HSCs. Mice were pretreated with PBS or rapamycin (Rapa) 2h before PBS or pI:C treatment. CD41 levels in HSCs were determined 16h after pI:C treament of mice. Data are presented as fold change in MFI, mean ±SEM are indicated, $n \geq 3$.

(K) Increased mTOR signaling in HSCs and MkPs upon inflammation. 16h after PBS or pI:C treatment of mice, levels of S6 ribosomal protein phosphorylation were determined by Phospho Flow. Left panel: Representative histogram showing pS6 signal in homeostatic HSC and 16h after pI:C treatment. Right panel: quantification of pS6 MFI. Data are presented as mean and SEM, $n \geq 3$ per group.

(L) Sca-1 is not involved in pI:C-induced CD41 up-regulation in HSCs. HSCs from PBS and pI:C treated WT and Sca-1$^{-/-}$ mice were analyzed for CD41 protein expression by flow cytometry (16h after injection). Data are presented as fold change in MFI, mean ±SEM are indicated, $n \geq 3$.

(M) TLR4/MYD88/TRIF signaling regulates LPS-induced Mk protein synthesis. HSCs from PBS and LPS treated WT, $TLR4^{-/-}$, $MYD88^{-/-}$, $TRIF^{-/-}$ and $IFNAR^{-/-}$ mice were analyzed for CD41 protein expression by flow cytometry (16h after injection). Data are presented as fold change in MFI, mean ±SEM are indicated, $n \geq 3$.

(N) Platelet depletion of mice induces only small changes in Mk protein expression. WT mice were treated with PBS, pI:C, PBS and platelet depletion antibody, or pI:C and platelet depletion antibody followed by analysis for CD41 protein expression by flow cytometry. Data are presented as fold change in MFI, mean ±SEM are indicated, $n \geq 3$.

In (G)-(N) significance was determined using an unpaired, two-tailed student's t test. * $p \leq 0.05$, ** $p \leq 0.01$, *** $p \leq 0.001$, **** $p \leq 0.0001$, NS: non-significant

Figure S2, related to Figure 2. Single-cell *ex vivo* Tracking of HSCs.

(A) Number of mature Mks formed at day 14 of culture of classical MkPs and HSCs forming '*Mk only*' colonies (i.e. SL-MkPs). Mean and SEM are indicated.

(B) Representative images of a large '*Mk only*' colony (top left), '*mixed*' colony (top right), MkP colony (bottom left), and 'myeloid only' colony (bottom right) at day 14 of culture.

(C) Kinetic analysis of the generation of immature (left panels), mature Mk (middle panels), and myeloid cells (right panel) from single-sorted LT-HSCs that gave rise to '*mixed*' colonies (upper panels) and '*Mk only*' colonies (lower panels). Single-sorted classical MkPs were included as a control. Data are presented as mean and SEM.

Significance was determined using a Mann–Whitney–Wilcoxon test. * $p \leq 0.05$, ** $p \leq 0.01$, *** $p \leq 0.001$, **** $p \leq 0.0001$, NS: non-significant

Figure S3, related to Figure 3. Inflammation Drives a Cellular Mk Maturation Program at Distinct Levels of Megakaryopoiesis.

(A) Electron microscopy analysis of $Lin^-cKit^+CD150^+CD48^-$ HSCs from PBS and pI:C treated mice as well as CD41low and CD41high HSCs from pI:C treated mice, 16h after treatment. MVBs are marked in red. One representative 60-nm section per cell and magnification of inset highlighted was investigated. MVBs are marked in red.

(B) Immunofluorescence microscopy analysis of total bone marrow (tBM), and $Lin^-cKit^+CD150^+CD48^-$ HSCs from PBS and CD41low and CD41high HSCs from pI:C treated mice, 16h after treatment. Cells were stained for platelet factor 4 (Pf4) and von willebrand factor (Vwf) and counterstained with DAPI (blue).

(C) Quantification of number of $Pf4^+$ and Vwf^+ granular structures of cells described in (B). Data are presented as mean ±SEM.

(D) Impact of mTOR, STAT1 and IFNAR signaling on cell size increase. Left panel: Mice were pretreated with PBS or rapamycin (Rapa) 2h before pI:C treatment. Right panel: Experiments were performed with WT, $STAT1^{-/-}$ and $IFNAR^{-/-}$ mice. Data are presented as mean ±SEM, $n \geq 3$.

(E) Granularity and cell size estimation using flow cytometric side scatter (SSC) and forward scatter (FSC) parameters. CD41 subpopulations of LT-HSCs from PBS and pI:C treated mice were analyzed for their SSC and FSC MFI. Data are presented as mean ±SEM, $n \geq 3$.

(F) Impact of mTOR, STAT1 and IFNAR signaling on polyploidy of MkPs. Left panel: Mice were pretreated with PBS or rapamycin (Rapa) 2h before pI:C treatment. Right panel: Experiments were performed with WT, $STAT1^{-/-}$ and $IFNAR^{-/-}$ mice. Data are presented as mean ±SEM, $n \geq 3$.

Significance was determined using a Mann–Whitney–Wilcoxon test in (C) and an unpaired, two-tailed student's t test (D), (E) and (F). * $p \leq 0.05$, ** $p \leq 0.01$, *** $p \leq 0.001$, **** $p \leq 0.0001$, NS: non-significant

Figure S4, related to Figure 4. Megakaryocytic Protein Up-regulation in HSCs is Mediated by a Post-Transcriptional Mechanism.

(A) Protein interaction network of significantly changed proteins of IFN response cluster, megakaryocyte and platelet cluster and Mk transcription factors**.** Protein and transcript levels are derived from proteomics and qPCR, respectively. Anti-correlation index defined as difference between transcript and protein log2 fold change ratios (from -2: high correlation (grey) to +5.5: high anti-correlation (yellow)).

(B) Platelet depletion of mice followed by induction of inflammation. Top panel: Representative FACS plots demonstrating the efficient depletion of platelets 2h after i.v. injection of GPIb antibody. RBC, Red Blood Cells; WBC, White Blood Cells. Bottom panel: 2h after platelet depletion, mice were injected with pI:C, and 16h later, Mk protein levels were determined by flow cytometry in HSCs. Data are presented as mean ± SEM with $n \geq 3$.

(C) Inflammation-induced translation correlates with increased CD41 expression in HSCs. O-propargyl-puromycin (OP-Puro) incorporation was measured 16h after PBS/pI:C and 1.5h after OP-Puro administration (see methods). Data are presented as mean ±SEM, $n \geq 3$.

(D) Pdcd4 and Eef2k down-regulation upon pI:C in HSCs. Left panel: Log2 fold changes of the translation inhibitors Pdcd4 and Eef2k in HSCs upon pI:C from proteomic data. Right panel: All proteins are displayed, Pdcd4 and Eef2k are highlighted in red. Data are presented as mean ±SEM, $n \geq 3$.

(E) Left panel: Illustration of ribosomal profiling. Right panel; 18S rRNA is highly enriched in the ribosomal fraction if compared to the cytosolic fraction. Data are presented as mean ±SEM, $n \geq 3$.

Significance was determined using an unpaired, two-tailed student's t test. * $p \leq 0.05$, ** $p \leq 0.01$, *** $p \leq 0.001$, **** $p \leq 0.0001$, NS: non-significant

Figure S5, related to Figure 5. HSCs Switch from a Stochastic to a Coordinated Mk Transcript Expression Program upon Commitment from Multipotency towards the Mk Lineage.

(A) Assessment of the transcriptional noise of Mk and platelet cluster genes and control genes in HSC subpopulations. The fano factor ($F = \sigma^2/\mu$, where σ^2 is variance and μ the mean expression of a transcript) was calculated from the single-cell qPCR data for the different CD41 subpopulations of HSCs and for MkPs. Fano factor calculations were performed for the Mk and platelet genes (top panel), for the interferon response genes (bottom panel, red) and for housekeeping genes (bottom panel, blue).

(B) Single-cell qPCR of Mk transcription factors of MkPs and LT-HSC CD41 subpopulations. Ct-values are displayed.

(C) Correlation heatmap of Mk transcription factors and Mk transcripts. Pearson correlation coefficients of Mk transcripts and Mk transcription factors were determined and displayed according to the indicated color code.

(D) Expression values of Mk transcription factors or Mk transcripts of MkPs and LT-HSC CD41 subpopulations. Representative gene pairs are shown. Expression values are presented as Ct-values.

(E) Technical noise fit and interference of highly variable genes of single-cell RNA-seq data. Mk and platelet cluster genes are enriched among the significantly highly variable genes in HSCs and progenitors (p-value: 0.001, Fisher's exact test). ERCC spike-ins were used to fit technical noise and infer the most variably expressed genes (see methods section and Brenecke et al.). CV^2, squared coefficient of variation

(F) Comparison of Mk transcript expression of VWF^+ HSCs, VWF^- HSCs and SL-MkPs. Single-cell qPCR data was binned into clusters with cells positive and negative for *Vwf* and compared to CD41high SL-MkPs of pI:C treated mice.

Significance was determined using a paired two-tailed student's t test (A). * $p \leq 0.05$, ** $p \leq 0.01$, *** $p \leq 0.001$, **** $p \leq 0.0001$, NS: non-significant.

Figure S6, related to Figure 6. The Most Potent and Primitive SL-MkPs Reside in a Dormant State and are Efficiently Activated upon Inflammation.

(A) H2B-GFP label-retention assay (LRC), control mice and control populations. Control mice and control populations of LRC experiment of figure 6A-D.

(B) Cell size (left panel) and granularity (right panel) estimations using FSC and SSC analysis of LRC and non-LRC $Lin^-cKit^+CD150^+CD48^-CD34^-$ LT-HSCs upon pI:C treatment. Experimental settings as in figure 5A-C.

(C) Cell cycle distribution of CD41 subpopulations of $Lin^-cKit^+CD150^+CD48^-$ HSCs measured by Ki67-Hoechst staining, 16h after treatment of mice with PBS, pI:C, LPS and TNFα. Data are presented as mean ±SEM, $n \geq 3$.

(D) Quantification of FoxO3a localization. Quantification of confocal microscopy images of indicated $Lin^-cKit^+CD150^+CD48^-CD34^-$ LT-HSCs CD41 subpopulations, 16h after treatment of mice with PBS or pI:C. Data are presented as mean ±SEM, $n \geq 3$.

(E) Cell cycle distribution of CD41 subpopulations of $Lin^-cKit^+CD150^+CD48^-$ HSCs measured by Ki67-Hoechst staining, 24h after treatment of mice with PBS or pI:C. Data are presented as mean ±SEM, $n \geq 3$.

Significance was determined using an unpaired, two-tailed student's t test. * $p \leq 0.05$, ** $p \leq 0.01$, *** $p \leq 0.001$, **** $p \leq 0.0001$, NS: non-significant

SUPPLEMENTAL TABLE LEGENDS

Table S1, related to Figure 1. PBS to pI:C proteomic data of WT and $IFNAR^{-/-}$ HSCs and progenitors. Proteomic data for all identified proteins.

SUPPLEMENTAL EXPERIMENTAL PROCEDURES

Mouse Strains

All animal experiments were approved by the Animal Care and Use Committees of the German Regierungspräsidium Karlsruhe für Tierschutz und Arzneimittelüberwachung. Mice were maintained in individually ventilated cages in the DKFZ animal facility. Wildtype (WT) mice (C57BL/6J or B6.SJL-Ptprc^{a} Pepc^{b}/BoyJ) were purchased from Harlan Laboratories or Charles River Laboratories, respectively. Female six to ten week old mice were used throughout the study. IFNAR$^{-/-}$ (Huang et al., 1993), STAT1$^{-/-}$ (Durbin et al., 1996), TLR4$^{-/-}$ (Poltorak et al., 1998), MYD88$^{-/-}$ (Adachi et al., 1998), TRIF$^{-/-}$ (Ermolaeva et al., 2008) (provided by M. Pasparakis), ACTB-dtTomato (Muzumdar et al., 2007) and SCL-tTA:H2B-GFP (Wilson et al., 2008) mice have been previously described.

Bone Marrow Preparation and Lineage Depletion

Bone marrow was prepared from femur, tibia, humerus, ilium, and columna vertebralis by crushing bones in RPMI-1640 medium (Sigma) supplemented with 2% FCS. For cell sorting, cells expressing the lineage markers CD11b (M1/70), Gr-1 (RB6.8C5), CD4 (GK1.5), CD8a (53.6.7), Ter119 (Ter119) and B220 (RA3-6B2) were depleted by incubation with rat monoclonal antibodies. Subsequently, cells were washed and incubated with anti-rat IgG-coated Dynabeads for 15 min (4,5µm supermagnetic polystyrene beads (Invitrogen), 1mL of beads / $3x10^{8}$ bone marrow cells). Cells expressing lineage markers were depleted using magnetic separation and the remaining lineage-negative cells were isolated.

Flow Cytometry and Cell Sorting

For flow cytometric analysis, bone marrow (BM) was prepared, cells were incubated with respective FACS-antibody mixes in RPMI-1640 supplemented with 2% FCS and stained for 30 min on ice. For Phospho-flow experiments, BM cells were stained with surface markers,

and fixed, permeabilized and stained using Phosflow Perm Buffer I and III (BD Biosciences) according to manufacturer's instructions. Cells were analyzed using LSRII and LSRFortessa flow cytometers equipped with 350nm, 405nm, 488nm, 561nm, and 640nm lasers (both BD biosciences). Data was analyzed using FlowJo (TreeStar). For FACS-sorting FACSAria I, II and III cell sorters (BD Biosciences) were used.

FACS Gating Strategy / Gating Without Sca-1

To compare populations between homeostasis and inflammation, populations were gated without stem cell antigen 1 (Sca-1), as it is highly up-regulated during inflammation. Gating of HSCs and committed progenitors was adapted from Kiel et al. (2005), Nakorn et al. (2003), Pronk et al. (2007), Wilson et al. (2008). If not indicated otherwise, populations were gated as follows, HSCs: $Lin^-cKit^+CD150^+CD48^-$; short-term HSCs: $Lin^-cKit^+CD150^+CD48^-CD34^+$; Long-term HSCs: $Lin^-cKit^+CD150^+CD48^-CD34^-$; GMPs: $Lin^-cKit^+Fc\gamma R^+$; MkPs: $Lin^-cKit^+Fc\gamma R^-CD150^+CD105^-CD9^{high}$**;** MEPs: $Lin^-cKit^+Fc\gamma R^-CD150^+CD105^-CD48^+$CD9low**;** CFU-E and Pro Ery: $Lin^-cKit^+Fc\gamma R^-CD150^-CD105^+$; Pre CFU-E: $Lin^-cKit^+Fc\gamma R^-CD150^+CD105^+$.

Even though cells were gated without Sca-1, $Lin^-cKit^+CD150^+CD48^-$ HSCs and $Lin^-cKit^+CD150^+CD48^-CD34^-$ long-term HSCs (LT-HSCs) were homogeneously positive for the HSC markers Sca-1, EPCR and ESAM, and negative for Flt3 and thus correspond to $Lin^-cKit^+CD150^+CD48^-Sca\text{-}1^+EPCR^+ESAM^+Flt3^-(CD34^-)$ cells (Figure S1A and S1B), whereas committed progenitors were Sca-1-negative (Figure S1C).

Cell Cycle Analysis

For Ki67-Hoechst cell cycle and ploidy analysis, surface stainings were performed as described. Subsequently, cells were fixed and permeabilized using cytofix-cytoperm buffer

(BD Biosciences) and incubated with Ki67 antibody (BD Biosciences) overnight at 4°C. Cells were stained with 25µg/mL Hoechst 33342 (Invitrogen) and analyzed.

For BrdU incorporation assays, mice were injected i.p. with 18mg/kg BrdU (Sigma), 12h prior to the experiment. BM was isolated as described and stained for surface markers. Subsequently, cells were fixed and BrdU staining was performed according to instructions of the BrdU Flow kit (BD Biosciences).

Measurement of the translational activity using OP-Puro

Measurement of the translational activity using O-propargyl-puromycin (OP-Puro) was performed as described before with minor differences (Signer et al., 2014). 14.5h after PBS or pI:C administration, mice were treated intraperitoneal with 50mg/kg OP-Puro. Bone marrow was harvested 16h after PBS/pI:C and1.5h after OP-Puro administration. Subsequently, cells were lineage-depleted, stained with surface markers, fixed with 1% paraformaldehyde in PBS for 15 min on ice and permeabilized in PBS supplemented with 0.1% saponin (Sigma) for 5 min at room temperature as described by Signer et al.. OP-Puro incorporation was visualized by following the instructions of the Click-iT Cell Reaction Buffer Kit (Life Technologies).

Bone Sections

8µm bone sections of frozen femurs were prepared using the Kawamoto tape method (Kawamoto, 2003) with minor differences. Briefly: Bones were excised from mice, fixed, decalcified and placed in sucrose prior to embedding in OCT and freezing. 8µm sections of frozen femurs were then cut using the Leica tape system, stained with indicated antibodies overnight at 4°C and images were acquired using an LSM710 microscope. Images were prepared using ImageJ software.

Single-Cell RNA sequencing

For amplification of cDNA and construction of libraries for paired-end sequencing, a slightly modified version of the QUARTZ-Seq protocol (Sasagawa et al., 2013) was used. In short, cells were sorted into 0.4µL lysis buffer containing 0.5% NP-40 and ERCC control RNA spike ins (Life Technologies) at a final dilution of 1:2.000.000 using a BD FACSAria II (BD Bioscience) under the single-cell mode. cDNA synthesis was primed using 0.8µL of priming buffer (1.5x PCR Buffer with MgCl2, 41.67nM RT primer (TATAGAATTCGCGGCCGCTCGCGATAATACGACTCACTATAGGGCGTTTTTTTTT TTTTTTTTTTTTTTT), 4U/µL RNAsin plus (Promega) and 50µM dNTPs). All other steps were performed exactly as described by Sasagawa et al. Libraries were then clustered and sequenced on an Illumina HiSeq 2000. Raw sequencing reads were aligned to the *Mus Musculus* genome (assembly GRCm38) to which the sequences of the ERCC spike-ins had been appended. HTSeq (Simon Anders et al., in revision) was used to obtain transcript count tables, which were further analyzed using R. In particular, we employed a published computational method to identify genes whose observed expression variability exceeds the variability caused by technical noise (Brennecke et al., 2013). Technical noise of the method was estimated by relying on the known concentration of ERCC control RNAs spiked into the reaction at the initial step. Principal component analysis (PCA) was used to cluster cells based on global patterns of gene expression. Typically, PCA is preceded by scaling of the individual variables to unit variance in order to avoid that variables measured on different scales affect the eigenvector decomposition differently. Here, however, such scaling would give equal weight to genes whose observed variance is mostly due to technical noise and to genes whose observed variance is predominantly biological. We therefore scale the read count n of gene j in cell i by

$$s_{ij} = \left(\log(n_{ij} + 0.1) - \frac{1}{L} \sum_{l=1}^{L} \log(n_{lj} + 0.1) \right) * v(\mu_j)^{-1/2}$$

where L is the number of cells, μ_j is the mean read count of gene j and $v(\mu_j)$ is the expected technical variance of a gene with expression μ_j, as defined by Brennecke et al.

Single-Cell qPCR

Single cells were sorted using a BD FACSAria II (BD Bioscience) under the single-cell mode. Cells were deposited directly into PCR-tubes loaded with 5µL RT/Taq-PCR master mix (1xCellsDirect reaction mix, Invitrogen; 0.1µM primer pool and 0.1µL RT/Taq enzyme mix, Invitrogen). Samples were immediately transferred to a PCR-machine. Sequence-specific reverse transcription (60 min, 50°C) was followed by reverse transcriptase inactivation / Taq polymerase activation (3min, 95°C), and 23 cycles of cDNA pre-amplification (15s 95°C, 15s 60°C, final elongation 15min 60°C). Pre-amplified samples were diluted 10-fold and 1µL was used for qPCR analysis utilizing *Power SYBR® Green* reagent (Applied Biosystems) on a ViiA™ 7 Real-Time PCR system (Applied Biosystems).

***Ex-Vivo* Single-cell Lineage Tracing**

Bone marrow was prepared, lineage-depleted and stained with FACS antibodies from mice 16 h after treatment with PBS or pI:C, as described above. Single cells were sorted into round bottom 96-well plates using a BD FACSAria III (BD Bioscience) under the single-cell mode into 10µL StemPRO34 (Sigma) supplemented with 10% pre-tested FCS, 100ng/mL mSCF, 100ng/mL mTPO, 10ng/mL mIL-3, 2U/mL hEPO, 2mM L-Gln, 50µM 2-me and 1% P/S. Cells were transferred into 1536-well plates, cultured for 14 days at 37°C and 5% CO2, and imaged daily using an AxioObserver Z1 (Zeiss) equipped with Spextra X fluorescence light source (Lumencor), motorized stage, Definitive Focus, Axiocam HRm, 0,4x TV adapter, 10x

FLUAR objective and single band pass filterset optimized for detection of Alexa-647 and PE. Culturing media was supplemented with 20ng/mL CD41-PE (BD Bioscience, 558040) and 100ng/mL custom labeled FcγR-a647 (eBioscience, 16-0161) antibodies, permitting a time-resolved identification of megakaryocyte and myeloid lineage commitment. Based on cell morphology and surface marker expression, colonies were classified as 'Mixed' colonies containing both mature megakaryocytes and myeloid cells, 'Myeloid only' colonies containing exclusively myeloid cells, and 'Mk only' colonies, consisting exclusively of mature Mks. Colony types that did not fall into any of these categories were designated as 'Others'. Cells were counted individually for 1-20 cells of each cell type, and were binned into 20-50, 50-100, 100-250, 250-1000 and >1000 cells categories for higher cell numbers. In such cases, cells falling into the mentioned bins were indicated as the lower end of the bin in figures (e.g. the 20-50 cell bin was indicated as 20, the 50-100 cell bin was indicated as 50 etc.). Using index–sorting, CD41 fluorescence intensity values from single-sorted HSCs were measured and retrospectively assigned to formed colonies.

Proteomics

Sample preparation for proteome analysis. $Lin^-cKit^+CD150^+CD48^-$ HSCs and $Lin^-cKit^+CD150^+CD48^+$ progenitors were FACS-sorted from WT and $IFNAR^{-/-}$ mice 16h after PBS or pI:C treatment and subjected to quantitative proteome analaysis in three (WT) and two ($IFNAR^{-/-}$) biological replicates into ice-cold PBS using the following parameters: 70 µm nozzle; 15,000 events/second; 35 psi. Sorted cells were collected into ice-cold PBS and stored at -80°C. Sort purity was >95% in all cases. Cell pellets corresponding to $4.5x10^5$ cells were lysed with 0.1% RapiGest (Waters) in 50 mM ammonium bicarbonate, then heated at 90ºC for 5 min, followed by sonication for 20 min and removal of cell debris by centrifugation. Cysteine disulfide bonds were reduced with 5 mM DTT for 30 min at 56ºC, alkylated with 10 mM iodoacetamide for 30 min at room temperature in the dark, followed by protein digestion

with sequencing grade modified trypsin (Promega) at 37ºC overnight. The reaction was stopped by adding TFA to a final concentration of 0.2% (v/v), and RapiGest was precipitated by further incubation at 37ºC for 45 min. Following centrifugation supernatants were collected and protein digests were stored at -20ºC until further use. Peptides of PBS- and pI:C condition were differentially labeled with stable isotope dimethyl labeling on column as previously described with slight modifications (Boersema et al., 2009). Briefly, SepPak C_{18} cartridges (Waters) were washed with ACN and conditioned with 0.1% (v/v) formic acid. Acidified samples were loaded and washed with 0.1% formic acid. Samples were labeled by flushing the columns with labeling reagent ('light' or 'heavy' using CH_2O (Fisher) + $NaBH_3CN$ (Fluka) or CD_2O (Isotec) + $NaBH_3CN$, respectively). After washing with 0.1% formic acid, labeled peptides were eluted with 80% (v/v) ACN/0.05% (v/v) formic acid. In a second (WT and $IFNAR^{-/-}$) and third (WT) biological replicate experiment, cell population reagents were swapped once, and the 'light' and 'heavy' labeled samples were mixed in 1:1 ratio based on total peptide amount. Samples were dried by vacuum centrifugation, reconstituted in IPG rehydration buffer and fractionated according to manufacturer's instructions using pH 3-10 IPG strips and 3100 OFFGEL fractionator (Agilent). The 12 fractions resolved were acidified and desalted with C_{18} Stagetips (Empore 3M) (Rappsilber et al., 2007). Peptide samples were dried by vacuum centrifugation and stored at -20ºC until further use.

LC-ESI-MS/MS analysis. In technical duplicates, peptides were separated using the nanoACQUITY UltraPerformance LC system (Waters) fitted with a trapping column (nanoAcquity Symmetry C_{18}, 5µm particle size, 180 µm inner diameter x 20 mm length) and an analytical column (nanoAcquity BEH C_{18}, 1.7µm particle size, 75µm inner diameter x 200 mm length). The outlet of the analytical column was coupled directly to an Orbitrap Velos Pro (Thermo Fisher Scientific) using a Proxeon nanospray source. The mobile phases for LC separation were 0.1% (v/v) formic acid in LC-MS grade water (solvent A) and 0.1% (v/v)

formic acid in ACN (solvent B). Peptides were first loaded with a constant flow of solvent A at 15 µL/min onto the trapping column. Trapping time was 2 min. Subsequently, peptides were eluted via the analytical column at a constant flow of 300 nL/min. During the elution step, the percentage of solvent B increased in a linear fashion from 3% to 7% in 10 min, then increased to 25% in 100 min and finally to 40% in a further 10 min. The peptides were introduced into the mass spectrometer via a Pico-Tip Emitter 360 µm OD x 20 µm ID; 10 µm tip (New Objective) and a spray voltage of 2.2 kV was applied. The capillary temperature was set at 230°C. Full scan spectra from *m/z* 300 to 1700 at resolution 30,000 FWHM (profile mode) were acquired in the Orbitrap MS. The filling time was set at maximum of 500 ms with limitation of 10^6 ions. From each full-scan spectra, the 15 ions with the highest relative intensity were selected for fragmentation in the ion trap. Normalized collision energy of 40% was used, and the fragmentation was performed after accumulation of 3 x 10^4 ions or after filling time of 100 ms for each precursor ion (whichever occurred first). MS/MS data was acquired in centroid mode. Only multiply charged (2+ and 3+) precursor ions were selected for MS/MS. The dynamic exclusion list was restricted to 500 entries with maximum retention period of 30 s and relative mass window of 7 ppm. In order to improve the mass accuracy, a lock mass correction using a background ion (m/z 445.12003) was applied. The mass spectrometry proteomics data have been deposited to the ProteomeXchange Consortium (Vizcaino et al., 2014) via the PRIDE partner repository with the dataset identifier PXD001500.

Protein identification and quantification. MS raw data files were processed with MaxQuant (version 1.2.2.5) (Cox and Mann, 2008). Enzyme specificity was set to trypsin/P and a maximum of two missed cleavages were allowed. Cysteine carbamidomethylation and methionine oxidation were selected as fixed and variable modifications, respectively. Methionine oxidation and protein N-terminal acetylation were selected as variable modifications. The derived peak list was searched using the built-in Andromeda search engine

(version 1.2.2.5) in MaxQuant against the Uniprot mouse database (2011.06.21) containing 53,623 proteins to which 248 frequently observed contaminants as well as reversed sequences of all entries had been added. Initial maximal allowed mass tolerance was set to 20 ppm for peptide masses, followed by 6 ppm in the main search, and 0.5 Dalton for fragment ion masses. The minimum peptide length was set to six amino acid residues and three labeled amino acid residues were allowed. A 1% false discovery rate (FDR) was required at both the protein level and the peptide level. In addition to the FDR threshold, proteins were considered identified if they had at least one unique peptide. The protein identification was reported as an indistinguishable "protein group" if no unique peptide sequence to a single database entry was identified. The 'match between runs' was enabled for consecutive peptide fractions with a 2 min time window. The iBAQ algorithm was used for estimation of the abundance of different proteins within a single sample (proteome) (Schwanhausser et al., 2011).

Proteomic bioinformatic analysis. For evaluation of differential protein expression between PBS and pI:C, statistical analysis was performed for the proteins quantified in at least two replicates using the Limma package in R/Bioconductor (Gentleman et al., 2004; Smyth, 2004). After fitting a linear model to the data, an empirical Bayes moderated t-test was used for the protein ratios. P-values were then adjusted for multiple testing with Benjamini and Hochberg's method and proteins with an adjusted p-value lower than 0.05 were considered to be differentially expressed between PBS and pI:C. Protein classification was performed using PANTHER classification system (Mi et al., 2007). Network analysis was done using STRING database (Jensen et al., 2009). Network visualization was performed in Cytoscape v2.8.3 (Shannon et al., 2003). For proteins with an adjusted p-value lower than 0.05, Gene Ontology (GO) enrichment analysis was performed using the functional annotation tool of DAVID (Huang et al., 2009). ggplot2 was used for visualization of results (Wickham et al. 2009). The interferon response cluster was determined by extracting the overlap of the significantly

changed proteins ($p_{adj} < 0.05$) of the HSC samples and the interferon response gene sets (Bosco et al., 2010; Browne et al., 2001). The megakaryocyte and platelet cluster was determined by calculating the overlap of the significantly changed proteins with highly expressed proteins (more than 4000 estimated copy numbers) of the platelet proteome (Burkhart el al., 2012) and with proteins of the platelet alpha granule proteome (Maynard et al., 2010).

Measuring Ribosome-Associated Transcript Abundance

The ribosome profiling approach was adapted and modified from Ingolia et al. (2012) using qPCR as a readout for transcript abundance. $1x10^7$ lineage-depleted bone marrow cells were lysed in 300µL ice-cold lysis buffer (1% (vol/vol) Triton X-100, 25U/ml, Turbo DNase I (Ambion), 20mM Tris·Cl (pH 7.5), 150mM NaCl, 5mM $MgCl_2$, 1mM DTT and 100µg/mL cycloheximide), incubated for 10 min on ice and triturated 10 times through a 26-G needle. The lysate was centrifugated for 10 min at 20.000g. The supernatant was underlayed with 700µL of 1M sucrose (in 20 mM Tris·Cl (pH 7.5), 150mM NaCl, 5mM $MgCl_2$, 1mM DTT and 100µg/ml cycloheximide, 20U/ml SUPERase·In RNase Inhibitor (Life Technologies)) and applied to ultracentrifugation using a TLS-55 rotor (Beckman Coulter) at 55.000 rpm at 4°C for 4h. RNA was extracted from the ribosomal pellet and from the cytosolic fraction by resuspension in 700µl Qiazol reagent (Qiagen), followed by incubation for 5 min on ice, vortexing for 5 min, and a second incubation for 5 min at 25°C. The RNA was extracted by adding chloroform and phase separation, followed by purification using the miRNAeasy kit (Qiagen) according to manufacturer's instructions. Transcripts were reverse transcribed by gene-specific reverse transcription using the SuperScript Vilo kit (Invitrogen) according to manufacturer's instructions. Relative transcript abundance of the ribosomal and cytosolic

fraction was determined by qPCR analysis of genes of interest and normalization to house keeping genes.

Electron Microscopy

Transmission electron microscopy was performed as described previously (Platani et al., 2009), with minor differences. Briefly, FACS-purified HSCs ($Lin^-cKit^+CD150^+CD48^-$) from 16h pI:C treated or PBS-treated mice were immobilized on poly-L-lysine coated coverslips for 30 min, fixed with 2.5% glutaraldehyde in cacodylate buffer (pH 7.2) for 30 min and stained with 1% osmium tetroxide for 40 min followed by 0.5% uranyl acetate staining. After dehydration in EtOH coverslips were dipped in propylene oxide and quickly placed on top of a BEEM capsule filled with Epon (Roth, Karlsruhe, Germany). Blocks were incubated at 60°C for 48 h. Serial sections were cut 60 nm thick and placed on a copper palladium slot grid coated with 1% Formvar (Serva Biochemicals, Paramus, NJ). Imaging was done on a CM120 Philips electron microscope. EM analysis was carried out in 100 cells both from PBS and pI:C treated cells. For cell size, grid intersection analysis in ImageJ was employed.

Immunofluorescence Microscopy

FACS-purified HSCs ($Lin^-cKit^+CD150^+CD48^-$) or LT-HSCs ($Lin^-cKit^+CD150^+CD48^-CD34^-$) from 16h pI:C treated or PBS-treated mice were immobilized on poly-L-lysine coated coverslips, fixed with cytofix-cytoperm buffer (BD Biosciences), blocked and stained with Foxo3a (Upstate), Vwf (Abcam) or Pf4 (Santa Cruz Biotechnology). Cells were counterstained with DAPI.

Statistics

If not indicated otherwise statistical analyses were performed using an unpaired, two-tailed student's t test or a Mann–Whitney–Wilcoxon test and results are presented as mean ± SEM

with n ≥ 3. For proteomics and single-cell RNAseq analysis p-values were adjusted for multiple testing using the Benjamini and Hochberg's method.

Data Analyses and Visualization

Gene expression data were analyzed and visualized using R packages (*scatterplot3d*, *beanplot*, *FactoMineR*, *VennDiagram* and custom-made scripts) and Prism. Heatmaps were generated using Multiple Experiment Viewer. Flow cytometry data were analyzed using FlowJo. Gene set enrichment analyses (GSEA) were performed and visualized using broad GSEA-software (Subramanian et al., 2005). For heatmap representation and GSEA of single-cell RNAseq data, the Mk and platelet cluster was defined as described above, except that the adjusted p-value of differential expressed proteins was increased to 0.1 to identify up-regulated proteins upon pI:C treatment. Gene Ontology (GO) analysis was performed using the functional annotation tool of DAVID (Huang et al., 2009).

SUPPLEMENTAL REFERENCES

Adachi, O., Kawai, T., Takeda, K., Matsumoto, M., Tsutsui, H., Sakagami, M., Nakanishi, K., and Akira, S. (1998). Targeted disruption of the MyD88 gene results in loss of IL-1- and IL-18-mediated function. Immunity *9*, 143-150.

Boersema, P.J., Raijmakers, R., Lemeer, S., Mohammed, S., and Heck, A.J. (2009). Multiplex peptide stable isotope dimethyl labeling for quantitative proteomics. Nature protocols *4*, 484-494.

Bosco, A., Ehteshami, S., Stern, D.A., and Martinez, F.D. (2010). Decreased activation of inflammatory networks during acute asthma exacerbations is associated with chronic airflow obstruction. Mucosal immunology *3*, 399-409.

Brennecke, P., Anders, S., Kim, J.K., Kolodziejczyk, A.A., Zhang, X., Proserpio, V., Baying, B., Benes, V., Teichmann, S.A., Marioni, J.C*., et al.* (2013). Accounting for technical noise in single-cell RNA-seq experiments. Nature methods *10*, 1093-1095.

Browne, E.P., Wing, B., Coleman, D., and Shenk, T. (2001). Altered cellular mRNA levels in human cytomegalovirus-infected fibroblasts: viral block to the accumulation of antiviral mRNAs. Journal of virology *75*, 12319-12330.

Cox, J., and Mann, M. (2008). MaxQuant enables high peptide identification rates, individualized p.p.b.-range mass accuracies and proteome-wide protein quantification. Nature biotechnology *26*, 1367-1372.

Durbin, J.E., Hackenmiller, R., Simon, M.C., and Levy, D.E. (1996). Targeted disruption of the mouse Stat1 gene results in compromised innate immunity to viral disease. Cell *84*, 443-450.

Ermolaeva, M.A., Michallet, M.C., Papadopoulou, N., Utermohlen, O., Kranidioti, K., Kollias, G., Tschopp, J., and Pasparakis, M. (2008). Function of TRADD in tumor necrosis factor receptor 1 signaling and in TRIF-dependent inflammatory responses. Nature immunology *9*, 1037-1046.
Gentleman, R.C., Carey, V.J., Bates, D.M., Bolstad, B., Dettling, M., Dudoit, S., Ellis, B., Gautier, L., Ge, Y., Gentry, J.*, et al.* (2004). Bioconductor: open software development for computational biology and bioinformatics. Genome biology *5*, R80.
Huang, D.W., Sherman, B.T., and Lempicki, R.A. (2009). Systematic and integrative analysis of large gene lists using DAVID bioinformatics resources. Nature protocols *4*, 44-57.
Huang, S., Hendriks, W., Althage, A., Hemmi, S., Bluethmann, H., Kamijo, R., Vilcek, J., Zinkernagel, R.M., and Aguet, M. (1993). Immune response in mice that lack the interferon-gamma receptor. Science *259*, 1742-1745.
Ingolia, N.T., Brar, G.A., Rouskin, S., McGeachy, A.M., and Weissman, J.S. (2012). The ribosome profiling strategy for monitoring translation in vivo by deep sequencing of ribosome-protected mRNA fragments. Nature protocols *7*, 1534-1550.
Jensen, L.J., Kuhn, M., Stark, M., Chaffron, S., Creevey, C., Muller, J., Doerks, T., Julien, P., Roth, A., Simonovic, M.*, et al.* (2009). STRING 8--a global view on proteins and their functional interactions in 630 organisms. Nucleic acids research *37*, D412-416.
Kawamoto, T. (2003). Use of a new adhesive film for the preparation of multi-purpose fresh-frozen sections from hard tissues, whole-animals, insects and plants. Archives of histology and cytology *66*, 123-143.
Kiel, M.J., Yilmaz, O.H., Iwashita, T., Yilmaz, O.H., Terhorst, C., and Morrison, S.J. (2005). SLAM family receptors distinguish hematopoietic stem and progenitor cells and reveal endothelial niches for stem cells. Cell *121*, 1109-1121.
Mi, H., Guo, N., Kejariwal, A., and Thomas, P.D. (2007). PANTHER version 6: protein sequence and function evolution data with expanded representation of biological pathways. Nucleic acids research *35*, D247-252.
Muzumdar, M.D., Tasic, B., Miyamichi, K., Li, L., and Luo, L. (2007). A global double-fluorescent Cre reporter mouse. Genesis *45*, 593-605.
Nakorn, T.N., Miyamoto, T., and Weissman, I.L. (2003). Characterization of mouse clonogenic megakaryocyte progenitors. Proceedings of the National Academy of Sciences of the United States of America *100*, 205-210.
Poltorak, A., He, X., Smirnova, I., Liu, M.Y., Van Huffel, C., Du, X., Birdwell, D., Alejos, E., Silva, M., Galanos, C.*, et al.* (1998). Defective LPS signaling in C3H/HeJ and C57BL/10ScCr mice: mutations in Tlr4 gene. Science *282*, 2085-2088.
Pronk, C.J., Rossi, D.J., Mansson, R., Attema, J.L., Norddahl, G.L., Chan, C.K., Sigvardsson, M., Weissman, I.L., and Bryder, D. (2007). Elucidation of the phenotypic, functional, and molecular topography of a myeloerythroid progenitor cell hierarchy. Cell stem cell *1*, 428-442.
Rappsilber, J., Mann, M., and Ishihama, Y. (2007). Protocol for micro-purification, enrichment, pre-fractionation and storage of peptides for proteomics using StageTips. Nature protocols *2*, 1896-1906.
Sasagawa, Y., Nikaido, I., Hayashi, T., Danno, H., Uno, K.D., Imai, T., and Ueda, H.R. (2013). Quartz-Seq: a highly reproducible and sensitive single-cell RNA sequencing method, reveals non-genetic gene-expression heterogeneity. Genome biology *14*, R31.
Schwanhausser, B., Busse, D., Li, N., Dittmar, G., Schuchhardt, J., Wolf, J., Chen, W., and Selbach, M. (2011). Global quantification of mammalian gene expression control. Nature *473*, 337-342.
Shannon, P., Markiel, A., Ozier, O., Baliga, N.S., Wang, J.T., Ramage, D., Amin, N., Schwikowski, B., and Ideker, T. (2003). Cytoscape: a software environment for integrated models of biomolecular interaction networks. Genome research *13*, 2498-2504.

Signer, R.A., Magee, J.A., Salic, A., and Morrison, S.J. (2014). Haematopoietic stem cells require a highly regulated protein synthesis rate. Nature *509*, 49-54.
Smyth, G.K. (2004). Linear models and empirical bayes methods for assessing differential expression in microarray experiments. Statistical applications in genetics and molecular biology *3*, Article3.
Subramanian, A., Tamayo, P., Mootha, V.K., Mukherjee, S., Ebert, B.L., Gillette, M.A., Paulovich, A., Pomeroy, S.L., Golub, T.R., Lander, E.S.*, et al.* (2005). Gene set enrichment analysis: a knowledge-based approach for interpreting genome-wide expression profiles. Proceedings of the National Academy of Sciences of the United States of America *102*, 15545-15550.
Vizcaino, J.A., Deutsch, E.W., Wang, R., Csordas, A., Reisinger, F., Rios, D., Dianes, J.A., Sun, Z., Farrah, T., Bandeira, N.*, et al.* (2014). ProteomeXchange provides globally coordinated proteomics data submission and dissemination. Nature biotechnology *32*, 223-226.
Wilson, A., Laurenti, E., Oser, G., van der Wath, R.C., Blanco-Bose, W., Jaworski, M., Offner, S., Dunant, C.F., Eshkind, L., Bockamp, E.*, et al.* (2008). Hematopoietic stem cells reversibly switch from dormancy to self-renewal during homeostasis and repair. Cell *135*, 1118-1129.

Figure S1

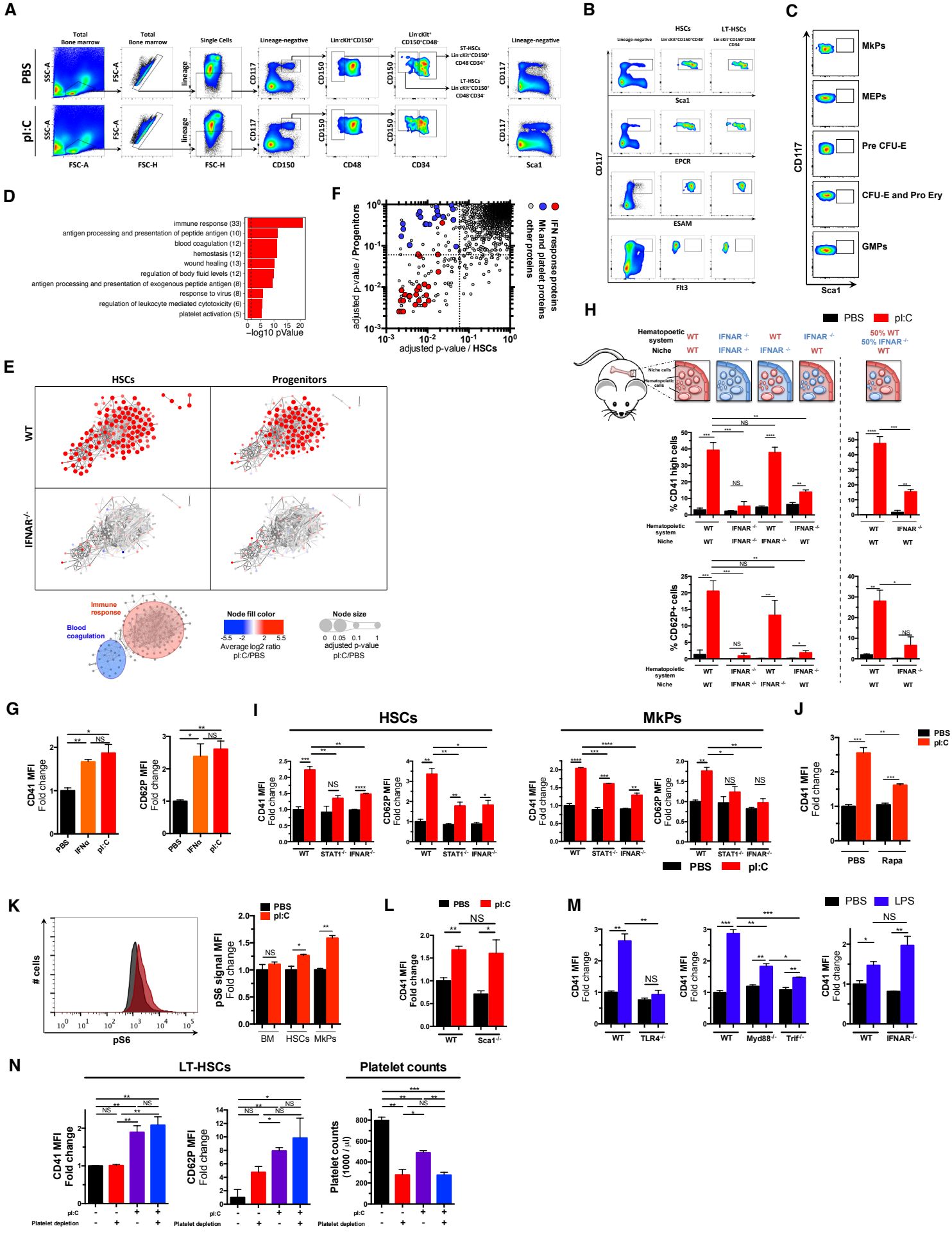
A
PBS
pI:C
Total Bone marrow
Single Cells
Lineage-negative
ST-HSCs Lin⁻cKit⁺CD150⁺ CD48⁻CD34⁺
LT-HSCs Lin⁻cKit⁺CD150⁺ CD48⁻CD34⁻
FSC-A
FSC-H
CD150
CD48
CD34
Sca1
B
HSCs
LT-HSCs
Sca1
EPCR
ESAM
Flt3
CD117
C
MkPs
MEPs
Pre CFU-E
CFU-E and Pro Ery
GMPs
D
immune response (33)
antigen processing and presentation of peptide antigen (10)
blood coagulation (12)
hemostasis (12)
wound healing (13)
regulation of body fluid levels (12)
antigen processing and presentation of exogenous peptide antigen (8)
response to virus (8)
regulation of leukocyte mediated cytotoxicity (6)
platelet activation (5)
−log10 pValue
F
adjusted p-value / Progenitors
adjusted p-value / HSCs
IFN response proteins
Mk and platelet proteins
other proteins
E
HSCs
Progenitors
WT
IFNAR-/-
Immune response
Blood coagulation
Node fill color
Average log2 ratio pI:C/PBS
Node size
adjusted p-value pI:C/PBS
H
PBS
pI:C
Hematopoetic system
Niche
50% WT 50% IFNAR-/-
% CD41 high cells
% CD62P+ cells
G
CD41 MFI Fold change
CD62P MFI Fold change
PBS
IFNα
pI:C
I
HSCs
MkPs
WT
STAT1-/-
IFNAR-/-
J
PBS
pI:C
Rapa
K
cells
pS6
pS6 signal MFI Fold change
BM
HSCs
MkPs
L
Sca1-/-
M
LPS
TLR4-/-
Myd88-/-
Trif-/-
N
LT-HSCs
Platelet counts
Platelet counts (1000 / µl)
pI:C
Platelet depletion

Figure S2

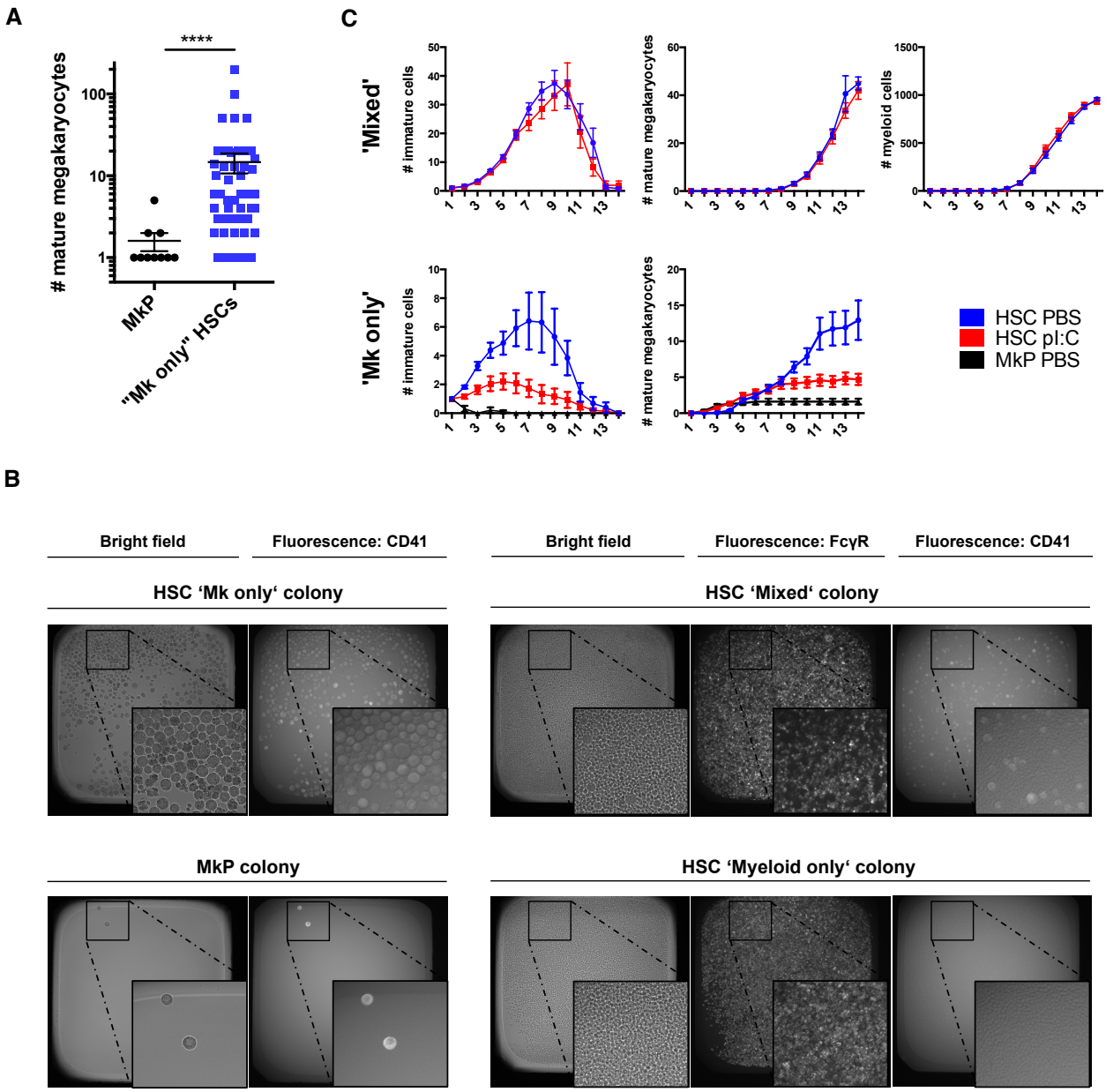
A
****
mature megakaryocytes
100
10
1
MkP
"Mk only" HSCs
C
'Mixed'
'Mk only'
immature cells
mature megakaryocytes
myeloid cells
HSC PBS
HSC pI:C
MkP PBS
B
Bright field
Fluorescence: CD41
Bright field
Fluorescence: FcγR
Fluorescence: CD41
HSC 'Mk only' colony
HSC 'Mixed' colony
MkP colony
HSC 'Myeloid only' colony

Figure S3

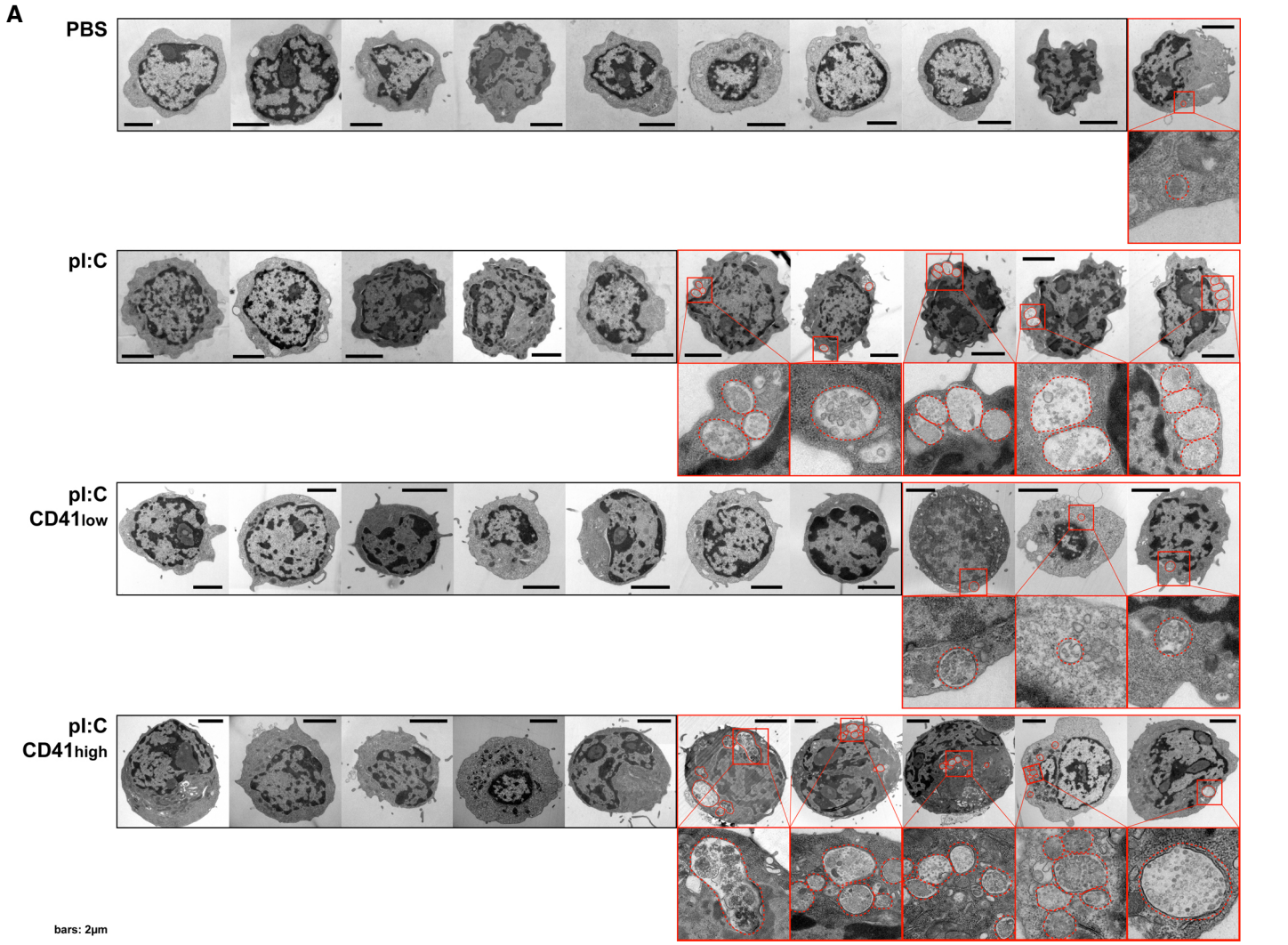
A
PBS
pI:C
pI:C CD41low
pI:C CD41high
bars: 2µm
B
Pf4
Vwf
untreated
-
pI:C CD41 low
pI:C CD41 high
bars: 2µm
C
Pf4+ granules
Vwf+ granules
ns
**
***
*
tBM
HSC
HSC pI:C low
HSC pI:C high
Treatment
CD41
D
FSC MFI
PBS
Rapa
pI:C
NS
WT
STAT1-/-
IFNAR-/-
E
LT-HSCs
PBS
pI:C
CD41
SSC
FSC
low/ med
high
PBS - CD41low/med
pI:C - CD41low/med
pI:C - CD41high
SSC MFI
FSC MFI
F
% polyploid MkPs
PBS
pI:C
NS
Rapa
WT
STAT1-/-
IFNAR-/-

Figure S4

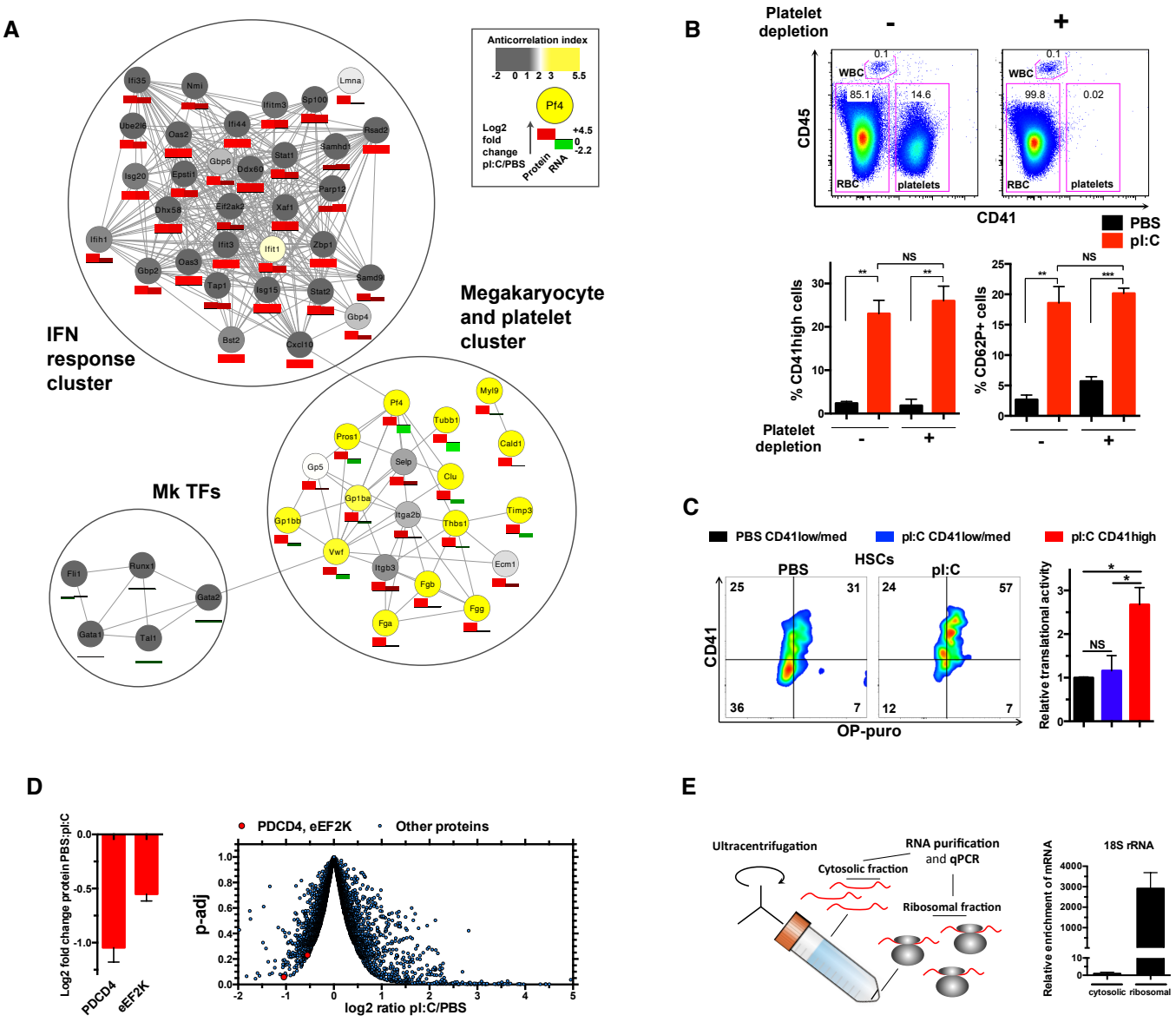
A
Anticorrelation index
-2 0 1 2 3 5.5
Pf4
Log2 fold change pI:C/PBS
Protein
RNA
+4.5
0
-2.2
IFN response cluster
Megakaryocyte and platelet cluster
Mk TFs
B
Platelet depletion
-
+
WBC
RBC
platelets
0.1
85.1
14.6
99.8
0.02
CD45
CD41
PBS
pI:C
% CD41high cells
% CD62P+ cells
NS
**
***
C
PBS CD41low/med
pI:C CD41low/med
pI:C CD41high
HSCs
PBS
pI:C
25
31
36
7
24
57
12
7
CD41
OP-puro
Relative translational activity
D
Log2 fold change protein PBS:pI:C
PDCD4
eEF2K
PDCD4, eEF2K
Other proteins
p-adj
log2 ratio pI:C/PBS
E
Ultracentrifugation
RNA purification and qPCR
Cytosolic fraction
Ribosomal fraction
18S rRNA
Relative enrichment of mRNA
cytosolic
ribosomal

Figure S5

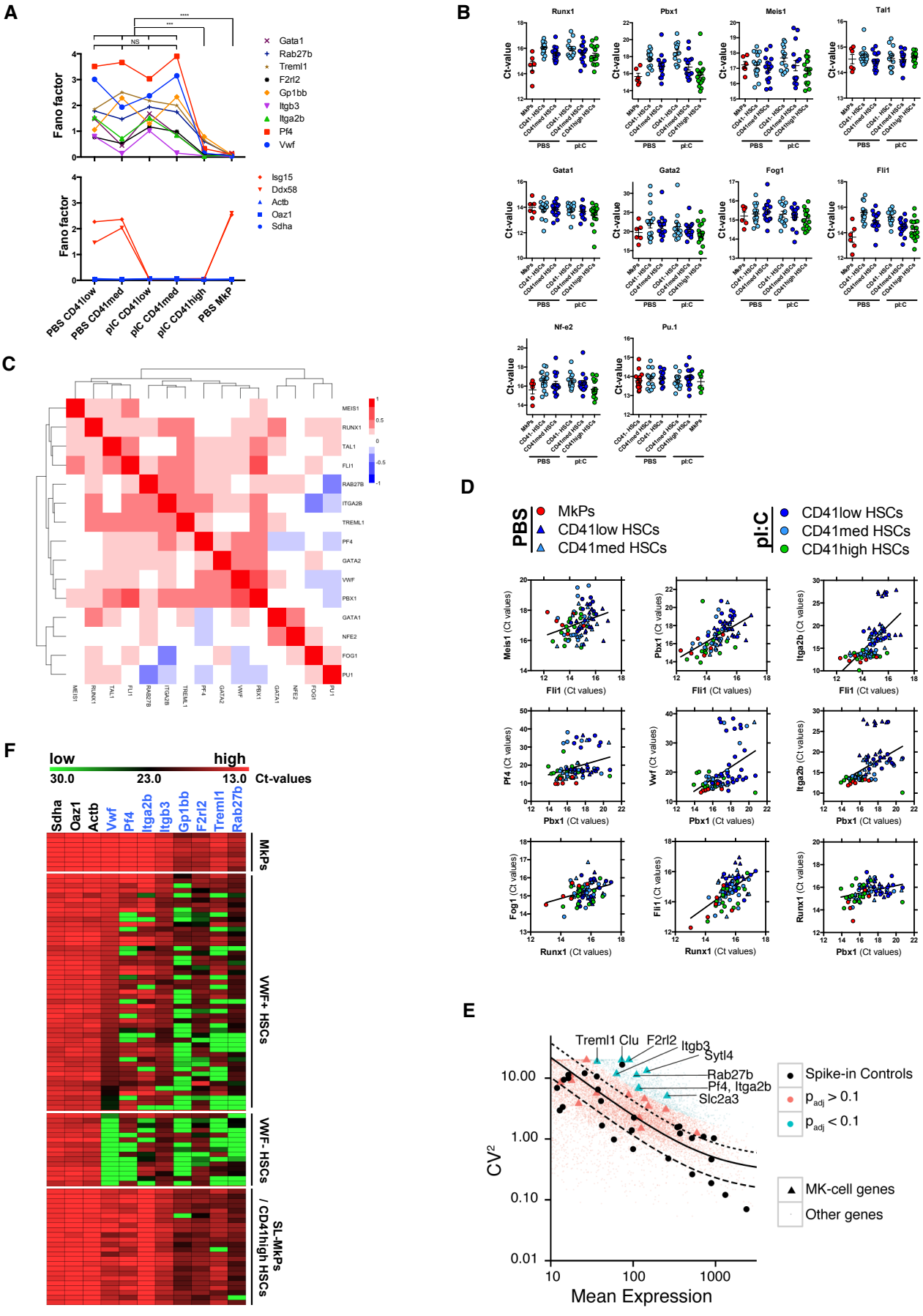
A
Fano factor
Gata1
Rab27b
Treml1
F2rl2
Gp1bb
Itgb3
Itga2b
Pf4
Vwf
Isg15
Ddx58
Actb
Oaz1
Sdha
PBS CD41low
PBS CD41med
pIC CD41low
pIC CD41med
pIC CD41high
PBS MkP
B
Runx1
Pbx1
Meis1
Tal1
Gata1
Gata2
Fog1
Fli1
Nf-e2
Pu.1
Ct-value
PBS
pI:C
C
D
PBS
MkPs
CD41low HSCs
CD41med HSCs
pI:C
CD41high HSCs
E
Treml1 Clu F2rl2 Itgb3
Sytl4
Rab27b
Pf4, Itga2b
Slc2a3
Spike-in Controls
MK-cell genes
Other genes
CV²
Mean Expression
F
low
high
30.0
23.0
13.0
Ct-values
MkPs
VWF+ HSCs
VWF- HSCs
SL-MkPs / CD41high HSCs

Figure S6

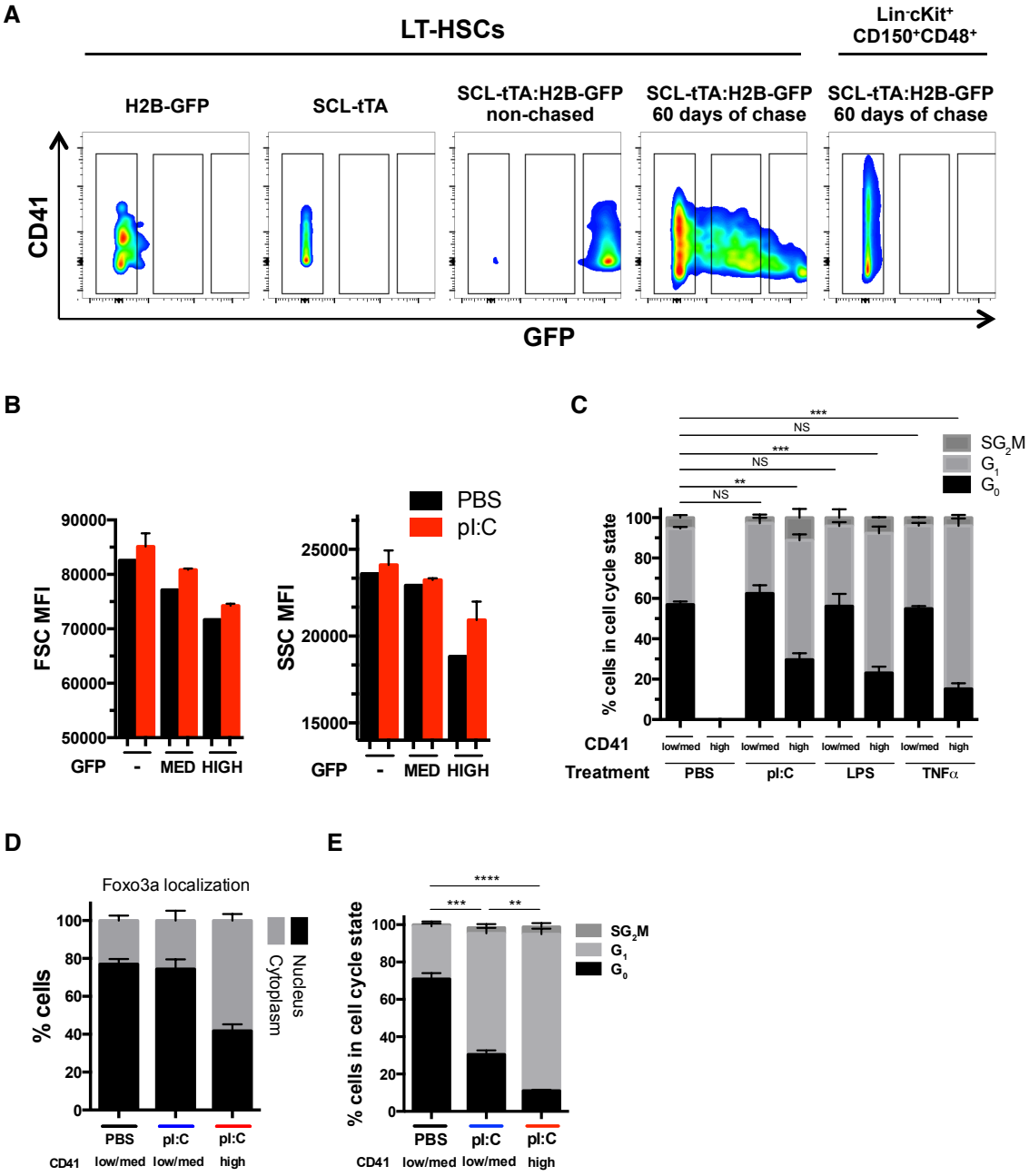
A
LT-HSCs
Lin-cKit+ CD150+CD48+
H2B-GFP
SCL-tTA
SCL-tTA:H2B-GFP non-chased
SCL-tTA:H2B-GFP 60 days of chase
SCL-tTA:H2B-GFP 60 days of chase
CD41
GFP
B
PBS
pI:C
FSC MFI
SSC MFI
GFP - MED HIGH
C
SG2M
G1
G0
% cells in cell cycle state
CD41
low/med high low/med high low/med high low/med high
Treatment
PBS pI:C LPS TNFα
NS
D
Foxo3a localization
% cells
Nucleus
Cytoplasm
PBS pI:C pI:C
CD41 low/med low/med high
E
% cells in cell cycle state
PBS pI:C pI:C
CD41 low/med low/med high